Title Page

Strawberry COP9 signalosome FvCSN5 regulates plant development and fruit ripening by facilitating polyamine oxidase FvPAO5 degradation to control polyamine and H_2O_2 homeostasis

Authors: Yun Huang[1#], Jiahui Gao[1#], Qinghua Wang[1], Guiming Ji[2], Wenjing Li[2], Yuanyue Shen[1], Jiaxuan Guo[2]*, Fan Gao[2]*

Running title: FvCSN5 controls polyamine and H_2O_2 homeostasis

Authors' Institutional Affiliation:

[1]Beijing Key Laboratory for Agricultural Application and New Technique, College of Plant Science and Technology, Beijing University of Agriculture, Beijing 102206, China;

[2]Key Laboratory for Northern Urban Agriculture of Ministry of Agriculture and Rural Affairs, Department of Resources and Environment, Beijing University of Agriculture, Beijing, China

Authors' email address:

Yun Huang: yunhuang@bua.edu.cn

Jiahui Gao: gjh696969@126.com

Qinghua Wang: qinghuasummer@163.com

Guiming Ji: 1074166581@qq.com

Wenjing Li: 17316112071@163.com

Yuanyue Shen: sfmn@tom.com

***Correspondence:** Fan Gao: gaofan@bua.edu.cn

Jiaxuan Guo: guojiaxuangjx@163.com

Telephone: 010-86-80727678

[#]These authors contributed equally to this work.

Abstract

Polyamines (PAs), including putrescine, spermidine, and spermine, are essential for plant growth and development. However, the post-translational regulation of PA metabolism remains elusive. Here, we report the COP9 signalosome subunit 5A (FvCSN5A)-mediated degradation of the PA oxidase FvPAO5 which catalyzes polyamines to produce H_2O_2. FvCSN5A was identified through a yeast two-hybrid screen using FvPAO5 as the bait. FvCSN5A localized in both the cytoplasm and nucleus, and its interaction with FvPAO5 occurred in the cytoplasm. *FvCSN5A* expression was ubiquitous in strawberries and peaked during fruit ripening. We utilized two independent RNAi lines, RNAi -1 and RNAi -2, in which *FvCSN5A* expression was downregulated by 8-fold and 46-fold, respectively, to demonstrate the pleiotropic roles of FvCSN5A. FvCSN5A positively regulated plant development, fertility, and fruit ripening by maintaining PA homeostasis, and promotes ubiquitination degradation of FvPAO5 through the interaction with cullin 1 (FvCUL1). The accumulation of FvPAO5 in the partial loss-of-function of FvCSN5A transgenic plants resulted from the inhibition of polyubiquitination modification of FvPAO5. Finally, we propose a post-translational regulatory mechanism involving the FvCSN5A-FvCUL1-FvPAO5 axis underlying PA and H_2O_2 homeostasis, providing novel insights into the regulation of plant growth by integrating the COP9 signalosome-mediated ubiquitination system into PA metabolism.

Introduction

Polyamines (PAs) are small polycationic molecules, primarily consisting of putrescine (Put), spermidine (Spd), and spermine (Spm). These molecules have been demonstrated to participate in numerous molecular processes, such as serving as a nitrogen storage pool (Siddappa and Marathe, 2020), protecting and stabilizing macromolecules (Napieraj et al., 2023), regulating reactive oxygen species (ROS) homeostasis (Pottosin et al., 2014; Jasso-Robles et al., 2020), and facilitating signal transduction (Gao et al., 2021). Consequently, PAs are essential for various aspects of plant development and growth, including photosynthetic regulation, secondary metabolism, flowering, fruit ripening, and environmental responses (Wang et al., 2019; Yu et al., 2019; Fortes et al., 2019; Gao et al., 2021; Aloisi et al., 2022; Navakoudis and Kotzabasis, 2022; Nandy et al., 2022; Blázquez, 2024). Despite the significant progress made in understanding PA metabolism and function, the regulatory mechanisms governing PA homeostasis at the post-translational level remain elusive.

In general, Put functions in photosynthetic protection, while Spd/Spm, especially Spm, are involved in ROS regulation. Spd, in particular, exhibits dual roles, acting as both a precursor and product in the interconversion between Put and Spm (Zhao et al., 2021; Zhong et al., 2023; Furumoto et al., 2024; Blázquez, 2024). In response to developmental and environmental stimuli, PA equilibria are fine-tuned at both the biosynthetic and degradative levels. PA biosynthesis begins with Put, catalyzed by either arginine decarboxylase (ADC) or ornithine decarboxylase (ODC). Put is then utilized as a substrate for the successive biosynthesis of Spd and Spm, catalyzed by Spd synthase (SPDS) and Spm synthase (SPMS), respectively, which require the addition of an aminopropyl group derived from decarboxylated S-adenosyl-L-methionine (dcSAM), generated from S-adenosyl-L-methionine (SAM) by SAM decarboxylase (SAMDC). (2) The degradation of PAs involves copper-containing diamine oxidase (CuAO/DAO)-mediated Put degradation, and flavin-containing polyamine oxidase (PAO)-mediated Spd/Spm degradation in a back-conversion (BC-type) or terminal-catabolism (TC-type) manner (Yu et al., 2019; Blázquez, 2024). Since PA decomposition produces H_2O_2 (Gupta et al., 2016; Yu et al., 2019), PA metabolism integrates the regulation of Put/Spd/Spm into H_2O_2, contributing to the fine-tuning of plant growth and development in response to environmental cues (Navakoudis and Kotzabasis, 2022; Zhan et al., 2023; Gao et al., 2024a).

It is noteworthy that AtPAO5 has been shown to participate in Arabidopsis xylem differentiation, regulated by auxin and cytokinin (Alabdallah et al., 2017), and OsPAO5 has been found to play an

76 important role in rice mesocotyl and seedling growth, as well as grain weight, grain number, and
77 yield potential, by producing H_2O_2 and ethylene (Lv et al., 2021). Additionally, an important advance
78 has been the elucidation of the role of PAO5 in strawberry fruit ripening as a negative regulator,
79 through the TC-type degradation of Spm/Spd and the concomitant production of H_2O_2 (Mo et al.,
80 2020). Given the continuously decreasing FaPAO5 protein levels during fruit ripening (Mo et al.,
81 2020), this observation prompts the consideration that ubiquitination-mediated degradation of PAO5
82 may represent a potential pathway for controlling both PA and H_2O_2 homeostasis.
83 As a common protein degradation pathway, the cullin-RING ubiquitin ligase (CRL) is widely found
84 in all eukaryotes, functioning in multiple cellular processes by the ubiquitin-mediated destruction of
85 target proteins dependent on an E1-E2-E3 cascade of the 26S proteasome system (Barry and Früh,
86 2006; Hotton and Callis, 2008). Specifically, the 76-amino-acid ubiquitin (UB) is covalently attached
87 to E1 (ubiquitin-activating enzyme) by ATP-derived adenylation, then the activated UB is
88 successively transferred onto E2 (ubiquitin conjugating enzyme) and substrate-E3 (ubiquitin ligase)
89 complex. A typical CRL consists of four parts: a cullin scaffold, a RING H2 Protein (RBX1) recruiter
90 of E2, and a substrate-E3 protein with an adaptor as a receptor for ubiquitylated peptides. In the E3
91 ligase superfamily, the activity of CRLs is regulated by RUB (related to ubiquitin-like protein) and
92 the COP9 signalosome (CSN; Hotton and Callis, 2008). As a component of the ubiquitin-proteasome
93 system, the CSN regulates CRL assembly by neddylation and deneddylation (Stratmann and
94 Gusmaroli, 2012). Notably, the CSN complex was originally identified by genetic screening of light-
95 induced-photomorphogenic mutants in Arabidopsis, revealing CSN functions in controlling CRL
96 activity and various cellular processes (Serino and Deng, 2003; Qin et al., 2020).
97 In the COP9 signalosome complex, CSN1-4, CSN7 and CSN8 contain a PCI (proteasome, COP9,
98 initiation factor 3) domain; CSN5, as a zinc-ion-activating metalloprotease, encompasses an MPN
99 (Mov34 and Pad1p N-terminal) domain and has two paralogs, CSN5A and CSN5B (Cope and
100 Deshaies, 2003; Verma et al., 2002; Gusmaroli et al., 2004; Wei and Deng, 2003; Jin et al., 2014).
101 Notably, CSN5A plays an important role in abscisic acid (ABA) signaling transduction by
102 controlling the protein stability of the bZIP transcription factor ABI5 (Jin et al., 2014). The MPN
103 domain is related to the activity of both CSN deneddylation and 26S-proteasome deubiquitination,
104 while the PCI domain is responsible for subunit interaction (Huang et al., 2005). The neddylation-

deneddylation cycle of CRL is involved in specific biological processes (Lingaraju et al., 2014; Reitsma et al., 2017; Liu et al., 2018; Mayor-Ruiz et al., 2019).

Given the ubiquitous presence of CRLs, the COP9 signalosome (CSN) also regulates the NEDD8 modification of certain CUL-based E3 ligases, such as SCF^{TIR1}, SCF^{SLY}, and SCF^{COI1}, facilitating the deneddylation of these CRLs in vivo (Qin et al., 2020). The E3 ubiquitin ligase SCF^{TIR1} directly interacts with the CSN, which is essential for the efficient degradation of its substrates in Arabidopsis (Schwechheimer et al., 2001). A more recent report indicates that the CSN-mediated deneddylation of CUL1 is necessary for the proper assembly of SCF^{EBF1} in Arabidopsis (Dong et al., 2024). CSN5 localizes in both the nucleus and cytosol, and functions in cleaving the NEDD8-CUL1 conjugate (deneddylation), a process implicated in protein degradation (Kwok et al., 1998; Lyapina et al., 2001; Schwechheimer et al., 2001). In fact, the CSN-mediated deneddylation not only prevents auto-ubiquitination of CRL components, but also facilitates the recycling of the cullin-RING heterodimer for numerous F-box/substrate interactions (Fischer et al., 2011). Intriguingly, a recent report indicates that CSN5 inhibits autophagy by regulating the ubiquitination of Atg6 (autophagy-related) and TOR (target of rapamycin), thereby mediating the pathogenicity of *Magnaporthe oryzae* (Shen et al., 2024). Collectively, the central role of CSN5 within the COP9 signalosome is involved in a wide range of cellular and biological processes, including light signaling, hormone signaling, and environmental responses in plants (Qin et al., 2020). However, whether the COP9 signalosome participates in polyamine (PA) metabolism remains unknown.

To explore a potential mechanism for the gradual decline in PAO5 levels during strawberry fruit development, we first screened for PAO5-interacting proteins using a yeast two-hybrid library screening approach. Notably, CSN5A was identified as a PAO5-interacting protein in two independent RNAi lines, RNAi -1 and RNAi -2. Subsequently, through a series of physiological, biochemical, and molecular analyses, we found that FvCSN5 regulates the protein stability of FvPAO5 via a ubiquitination-mediated degradation pathway, which in turn affects the homeostasis of polyamines, auxin, and H_2O_2, essential for strawberry plant growth, fertility, and fruit ripening. Finally, based on the available data and our current results, we propose a post-translational regulation model for PA and H_2O_2 homeostasis, regulated by the FvCSN5A-FvCUL1-FvPAO5 axis, providing novel insights into the integration of the COP9 signalosome into PA metabolism. This opens up an

attractive avenue for agricultural practices aimed at improving crop yield and quality through the manipulation of the CSN5-PAO5 pair.

Results

Identification of FvCSN5A as FvPAO5 interacting protein

Given the continual decrease in FaPAO5 protein levels during fruit ripening (Mo et al., 2020), it is plausible that FaPAO5 may be regulated through protein degradation. To investigate this hypothesis, we performed a yeast two-hybrid (Y2H) screen using FvPAO5 (FvH4_7g01430) as the bait. As a result, we identified an interacting protein of FvPAO5, designated as FvCSN5A (FvH4_2g36890), which is homologous to the Arabidopsis CSN5A protein (Fig. 1A). We subsequently validated the physical interaction between FvPAO5 and FvCSN5A using a variety of complementary experimental approaches. In the GST pull-down assay conducted in vitro, the FvPAO5-GST fusion protein was precipitated by His-FvCSN5A (Fig. 1B). Furthermore, the firefly luciferase complementation (FLC) assay revealed a strong fluorescent signal upon co-transformation of the FvPAO5-NLUC and FvCSN5A-CLUC constructs in tobacco leaves, while no such signal was observed in the control (Fig. 1C). To corroborate the in vivo interaction, we performed co-immunoprecipitation (CoIP) experiments by co-expressing MYC-tagged FvCSN5A with either FvPAO5-GFP or GFP alone in *Nicotiana benthamiana* epidermal cells via Agroinfiltration. The results demonstrated that MYC-FvCSN5A could specifically associate with FvPAO5-GFP, but not with GFP alone, indicating that FvPAO5 interacts with FvCSN5A in planta (Fig. 1D).

Finally, we employed a bimolecular fluorescence complementation (BiFC) assay to further validate the FvCSN5A-FvPAO5 interaction in plant cells. The FvPAO5-YNE (N-terminal of YFP) and FvCSN5A-YCE (C-terminal of YFP) constructs were delivered into *N. benthamiana* leaf cells, and distinct fluorescence was observed in the cytosolic localization, providing additional evidence for the interaction between FvPAO5 and FvCSN5A (Fig. 1E). Collectively, these complementary experimental results provide consolidated evidence that FvPAO5 interacts with FvCSN5A both in vitro and in vivo.

The expression pattern and subcellular localization of FvCSN5A

To explore the expression pattern of *FvCSN5A*, we tracked its transcriptional level in different organs of strawberry plants and across five developmental stages of strawberry fruit using RT-qPCR. The expression of *FvCSN5A* was highest in roots, followed by red seeds, stems, and leaves, while it was lowest in flowers and fruits (Fig. 2A). The *FvCSN5A* transcript level increased gradually from the white (Wt) to partial red (PR) stage and reached a peak during the full red (FR) stage (Fig. 2B). In contrast, the expression of *FvPAO5* decreased rapidly from the small green (SG) to FR stage (Mo et al., 2020). These results suggest that FvCSN5A may exert an effect on the fruit ripening process, potentially related to the decreased FvPAO5 levels.

To determine the subcellular localization of FvCSN5A, we expressed the Super1300:FvCSN5A-GFP construct or the empty vector (expressing GFP alone) in tobacco leaves and performed fluorescence imaging observations. The results showed that the FvCSN5A-GFP signals were detectable in both the cytoplasm and the nucleus, the latter of which overlapped with the 4',6-diamidino-2-phenylindole dihydrochloride (DAPI) staining, a dye used to label nuclei (Fig. 2C). In comparison, FvPAO5 was localized in the nucleus and peroxisomes, as evidenced by its co-localization with the peroxisome marker px-RK/CD3-983 (Fig. 2C). Given the finding in Fig. 1E that FvCSN5A and FvPAO5 interact in the cytosol, the interaction between these two proteins may promote the localization of FvPAO5 in the cytoplasm.

Inhibition of *FvCSN5A* expression led to developmental defects in leaves and flowers

CSN5 has been found to participate in crucial biological functions, such as development and stress response, in Arabidopsis and tomato (Shang et al., 2019; Qin et al., 2020); however, the function of the strawberry homolog FvCSN5A remains unknown. To elucidate the role of FvCSN5A, we generated RNAi-based FvCSN5A-knockdown *F. vesca* plants. Two independent transgenic lines exhibiting different levels of *FvCSN5A* expression were obtained and verified by red fluorescence (Fig. 3A; Fig. S1). The expression of *FvCSN5A* in the RNAi -1 and RNAi -2 lines was decreased by approximately 8-fold and 46-fold, respectively (Fig. 3B). The RNAi plants displayed typical trifoliate leaves, but exhibited abnormal petal and sepal morphologies (Fig. 3C-F). Specifically, the petal edges of *FvCSN5A* RNAi -1 and RNAi -2 plants appeared serrated, and many showed leaf-like sepals (Fig. 3E-F).

The RNAi plants maintained a similar leaf shape index and number of serrations compared to the wild-type leaves (Fig. 3G-H). However, the leaves of *FvCSN5A* RNAi -1 and *FvCSN5A* RNAi -2 plants exhibited deeper serrations with sharper serrated blade angles (Fig. 3I). Moreover, the petal and sepal numbers of the RNAi plants exhibited significant variation. In the wild-type, each flower typically has 10 to 14 sepals and 5 petals (Fig. 3J-K). In contrast, some flowers of the *FvCSN5A* RNAi plants had 6 to 9 sepals (6% in RNAi -1 and 44% in RNAi -2) and 4 petals (11% in RNAi -1 and 28% in RNAi -2), while the wild-type did not show such variation (Fig. 3J-K). Collectively, the reduction in *FvCSN5A* expression resulted in substantial developmental defects in both leaves and flowers.

FvCSN5A affected the fertility of strawberries, especially pollen viability

Since plant flowering and seed formation are fundamental to fruit development (Liao et al., 2018), we examined the influence of FvCSN5A on both floral organ and seed development. The *FvCSN5A* RNAi -1 and *FvCSN5A* RNAi -2 transgenic plants exhibited no observable defects in the appearance of the stigmas, carpels, or stamens (Fig. 4A-B). However, the number of carpels and anthers was reduced in *FvCSN5A* RNAi flowers (Fig. 4C-D).

Subsequently, we performed Alexander staining and in vitro pollen germination assays to assess pollen viability (Fig. 4E-H). Based on Alexander staining, we determined that there was near-complete pollen activity abortion in the lower expression line (*FvCSN5A* RNAi -2) (10.29±0.98) and a subtle reduction in the moderate expression line (*FvCSN5A* RNAi -1) (91.35±1.22) (Fig. 4G). A significant decrease in pollen germination in vitro was observed in *FvCSN5A* RNAi -1 (65.93±7.07) and *FvCSN5A* RNAi -2 (8.49±2.42) compared to the wild type (96.97±3.03) (Fig. 4H). Furthermore, the germinated pollen tube length of *FvCSN5A* RNAi plants was shorter than that of the wild type (Fig. 4I). These results demonstrate that the inhibition of *FvCSN5A* expression leads to reduced pollen viability in strawberry.

To further investigate the relative influence of male and female gametophytes on seed formation and fruit expansion, we performed reciprocal crosses between wild-type and *FvCSN5A* RNAi -2 plants. As shown in Fig. S2, more seeds were produced, and fruit expanded to a greater extent when wild-type pollen was applied to *FvCSN5A* RNAi -2 stigmas, compared to using *FvCSN5A* RNAi -2 as the

paternal plant. Collectively, these data indicate that FvCSN5A is essential for strawberry reproductive success, with a particular importance for pollen development.

FvCSN5A positively regulated fruit ripening

To gain insight into the function of FvCSN5A on fruit ripening, we observed the fruit coloring phenotype of *FvCSN5A* RNAi. The results demonstrated that strawberry fruit coloration was retarded in *FvCSN5A* RNAi -1 plants (Fig. 5A), while *FvCSN5A* RNAi -2 fruits were impeded from completing the normal development and maturation process (Fig. S3). The content of anthocyanin was lower in *FvCSN5A* RNAi -1 fruits compared to the control, consistent with the observed phenotype (Fig. 5B). The firmness analysis also revealed that the softening process was inhibited in *FvCSN5A* RNAi fruits (Fig. 5C). The fresh weight was further determined, indicating that the fresh weight of *FvCSN5A* RNAi fruits was smaller than that of the control (Fig. 5D). The contents of sucrose, glucose, fructose, and total soluble sugar were significantly lower in fruits of *FvCSN5A* RNAi (Fig. 5E).

The expression of genes related to sugar and anthocyanin accumulation, fruit softening, and PA homeostasis in transgenic strawberry fruits was also examined using RT-qPCR. The expression of sucrose transporter *FvSUT1*, coloring-related genes *FvCHS* and *FvANS*, firmness-related genes *FvPG* and *FvCEL* were significantly inhibited in the RNAi fruits, while sucrose synthase *FvSS*, which negatively regulates sugar accumulation, was elevated (Fig. 5F). Based on the expression of these marker genes, the physiological results, and phenotypic observations, these findings indicate that FvCSN5A regulated fruit ripening and fruit quality.

To explore the effect of FvCSN5A on PAs metabolism, the relative gene expression in WT and *FvCSN5A* RNAi fruits were detected. The results showed that the expression levels of polyamine synthetase (*FvADC1*, *FvSAMDC1*, *FvSPDS*, and *FvSPMS*) and polyamine oxidase (*FvPAO5*) in *FvCSN5A* RNAi fruits were significantly lower than those in WT.

To further verify the role of strawberry CSN5A, we manipulated *FaCSN5A* expression in octoploid strawberry fruits by overexpression or RNAi construction transiently transformation. The phenotype and RT-qPCR analysis demonstrated that the fruits with lower *FaCSN5A* mRNA level (*FaCSN5A* RNAi) colored slowly compared to the control fruits, while the fruits with higher *FaCSN5A* mRNA level (*FaCSN5A* OE) colored rapidly (Fig. S4A-B). The anthocyanin, soluble sugar, firmness and

their relative gene expression were detected and significantly changed in *FaCSN5A* OE and RNAi fruits (Fig. S4C-D). We also examined the expression of polyamine metabolism-related genes in control fruits, *FaCSN5A* RNAi and *FaCSN5A* OE transgenic fruits. The results showed that the expression levels of *FaADC1*, *FaSAMDC1*, *FaSPDS*, *FaSPMS*, and *FaPAO5* in *FaCSN5A* RNAi fruits were significantly lower than those in WT. The expression levels of these genes in *FaCSN5A* OE fruits were significantly higher than those in WT (Fig. S4D). Collectively, these results demonstrate that strawberry CSN5A controls fruit ripening as a positive regulator at both physiological and molecular levels.

FvCSN5A promoted FvPAO5 ubiquitination degradation

The CSN (COP9 signalosome) complex typically regulates plant development and stress response by modulating the cullin-RING E3 ubiquitin ligase complex. Therefore, we proposed that the FvCSN5A-FvPAO5 interaction might affect FvPAO5 protein stability and regulate strawberry development and fruit ripening.

Firstly, we investigated whether FvPAO5 was degraded in a cell-free system (Fig. 6A). The results showed that the protein level of FvPAO5 decreased when incubated with strawberry total protein, and the degradation was inhibited by the addition of the proteasome inhibitor MG132 (Fig. 6A). The accumulation of FvPAO5 was also assessed in *FvCSN5A* RNAi and wild-type (WT) plants. The accumulation of FvPAO5 was reduced in the wild-type plants, and showed a relatively higher level in the *FvCSN5A* RNAi plants compared to the WT plants (Fig. 6B). These data indicate that FvCSN5A may promote the degradation of FvPAO5 through ubiquitination.

The polyubiquitination of FvPAO5 was assessed in the *FvCSN5A* RNAi and WT plants. Tissue culture seedlings of *FvCSN5A* RNAi and WT were treated with or without 50 μM MG132 for 5 hours and then harvested for protein extraction. The ubiquitination-modified proteins were enriched with P62-agarose, and ubiquitinated FvPAO5 was detected by an anti-FvPAO5 antibody. Without MG132 treatment, polyubiquitinated FvPAO5 was weak in the WT plants, while it became significantly stronger under MG132 treatment. However, the FvPAO5 polyubiquitination signal was hardly visible in the *FvCSN5A* RNAi plants, regardless of whether MG132 was used or not (Fig.

6C). These data suggested that FvCSN5A promoted the proteasome-dependent degradation of FvPAO5 in an ubiquitin-mediated manner.

FvCSN5A interacted with FvCUL1 and maintained its stability

Many studies reported that CSN interacted with CUL1 in SCF-type E3s, and the deneddylation of the AtCUL1 was blocked in *atcsn* mutant (Schwechheimer et al., 2001; Cope and Deshaies, 2003; Gusmaroli et al., 2004). In strawberries, the *FvCUL1* transcripts level was highest in the root, and lowest in flowers (Fig. 7A). During fruit ripening, the expression pattern of *FvCUL1* was similar to *FvCSN5A*, rising fast and reaching the top at the FR stage (Fig. 7B). Therefore, we suspected that FvCSN5A would deneddylate FvCUL1 and enhance E3 ubiquitin ligase-mediated biological processes such as 26S protein ubiquitinated degradation.

To examine this point, we investigated the interaction between FvCUL1 (FvH4_2g25090) and FvCSN5A. The results showed that FvCUL1 was able to interact with FvCSN5A in Y2H and FLC assays (Fig. 7C-D). We also tested the influence of FvCSN5A on FvCUL1 protein level using anti-FvCUL1 antibody. We found the deneddylated and neddylated forms of FvCUL1 in wild-type, and the FvCUL1 protein level in the *FvCSN5A* RNAi markedly decreased (Fig. 7E). These results suggested that FvCSN5A as a subunit of CSN is essential for the deneddylation of FvCUL1, which may affect the protein stability of FvCUL1 and SCF E3 ubiquitin ligase activity.

Polyamine, phytohormone, and H_2O_2 level changed in the *FvCSN5A* RNAi plants

Previous studies have reported that CSN5A is involved in numerous phytohormone signaling pathways, including those mediated by the plant hormones IAA, JA, and GA (Jin et al., 2014; Qin et al., 2020). In the current investigation, we have determined that FvCSN5A promotes the ubiquitin-mediated degradation of FvPAO5, a key enzyme that catalyzes the conversion of spermidine (Spd) and spermine (Spm) to generate H_2O_2 (Mo et al., 2020). To elucidate the regulatory roles of FvCSN5A, we assessed the alterations in endogenous polyamines, phytohormones, and H_2O_2 generation in FvCSN5A RNAi plants.

Firstly, we quantified the levels of the three most abundant polyamines in strawberry-Spd, Spm, and putrescine (Put). The contents of Spd and Spm were significantly lower in *FvCSN5A* RNAi plants compared to wild-type (WT), with Spd being almost undetectable in *FvCSN5A* RNAi -2 (Fig. 8A-B). However, Put accumulation varied, being reduced in *FvCSN5A* RNAi -1 but not significantly different from WT in *FvCSN5A* RNAi -2 (Fig. 8C). These results indicate that the inhibition of

strawberry *FvCSN5A* expression leads to a substantial decrease in Spd and Spm levels, which may be attributable to the over-accumulation of the FvPAO5 protein.

Secondly, we investigated the contents of phytohormones related to plant development and environmental responses, including IAA, ABA, JA, GA, cytokinins (CK), and salicylic acid (SA). The synthesis of IAA, ABA, and JA was suppressed in *FvCSN5A* RNAi plants, with IAA displaying an 83% reduction (Fig. 8D-F). In strawberry, the most abundant GA compound was GA3, and the predominant CK compounds were TZR and DHZR. Interestingly, the levels of GA3, TZR, DHZR, and SA were elevated in *FvCSN5A* RNAi plants (Fig. 8G-I).

Finally, we assessed the amount of H_2O_2 in the *FvCSN5A* RNAi plants. The DAB staining results showed that the pollen grains and leaves of *FvCSN5A* RNAi plants, particularly *FvCSN5A* RNAi-2, were stained more intensely, indicating higher H_2O_2 levels, compared to the lighter staining observed in wild-type (Fig. 9A-B). Furthermore, the ROS generation, as detected by 2,7-dichlorodihydrofluorescein diacetate (DCFH-DA) fluorescence, was markedly higher in the pollen grains and leaves of *FvCSN5A* RNAi plants (Fig. 9C-D). The content analysis also confirmed that *FvCSN5A* RNAi plants had significantly elevated H_2O_2 production compared to wild-type (Fig. 9E). Collectively, these results indicate that the reduction of *FvCSN5A* expression leads to a significant decrease in the contents of polyamines and auxin, accompanied by an excessive accumulation of H_2O_2. The disruption of this homeostatic balance in *FvCSN5A* RNAi plants may contribute to the observed growth defects, retarded fruit ripening, and poor fertility phenotype.

DISCUSSION

Strawberry, as a perennial herbaceous plant, has emerged as a model organism for investigating the non-climacteric fruit ripening process, which is regulated by the intricate crosstalk of polyamines (PAs) with abscisic acid (ABA), indole-3-acetic acid (IAA), and ethylene (Guo et al., 2018; Bai et al., 2021; Gao et al., 2021). Aligned with the earlier postulation of "no growth, no PA production" (Russell, 1973), the present data not only further corroborate the pivotal role of PAs in fruit ripening, but also provide novel insights into the efficacy of PAs in modulating plant growth, flowering, as well as fruit yield and quality in strawberry. This is particularly evident through the first-time

identification of the FvCSN5-FvPAO5 module, which underscores the significance of the COP9 signalosome-ubiquitination system in PA metabolism.

Spd/Spm plays essential roles in strawberry vegetative and reproductive growth

Our previous investigations have demonstrated that during strawberry fruit development, putrescine (Put) content gradually declined, reaching its nadir in the ripe fruit, while spermidine (Spd) content also remained at low levels, albeit exhibiting a slight rise in the ripe fruit (Guo et al., 2018). Remarkably, spermine (Spm) content rapidly increased at the onset of ripening, becoming the dominant polyamine (PA) component in the ripe fruit. This corroborates the pivotal role of Spd/Spm, particularly Spm, in the ripening process, which is consistent with the abundance of FaSAMDC1 (Guo et al., 2018). Concomitantly, the protein expression levels of FaPAO5 gradually decreased during strawberry fruit development, indicating its function as a negative regulator of ripening, in alignment with the observed patterns of FaPAO5 and H_2O_2 amounts (Mo et al., 2020). These prior reports have revealed that the enhanced FaSAMDC and diminished FaPAO5 levels not only synergistically promote Spd/Spm accumulation, but also contribute to the production of FaPAO5-derived H_2O_2, suggesting a cooperative interplay between PAs and reactive oxygen species (ROS). Indeed, the expression of *OsPAO5* in rice seedlings is induced by light and suppressed by darkness, and *ospao5* mutants exhibit lower H_2O_2 levels, resulting in a longer mesocotyl, faster seedling growth, and improved yield (Lv et al., 2021). However, the post-translational regulation of PAO5 remains elusive.

Fortunately, an interactor of FvPAO5, FvCNS5A, has now been identified through a comprehensive suite of physiological, biochemical, and molecular evidence. Notably, *FvCNS5A* RNAi plants exhibited elevated levels of both FvPAO5 and H_2O_2 (Fig. 6 and 9) and reduced amounts of indole-3-acetic acid (IAA), abscisic acid (ABA), and jasmonic acid (JA), particularly a striking 83% decrease in IAA (Fig. 8), ultimately impairing plant growth, flowering, and fruit yield and ripening (Fig. 3-5). Intriguingly, the contents of Spd and Spm were significantly lower in the RNAi plants, with Spd being almost undetectable in the RNAi -2 line (Fig. 9), while Put levels remained unchanged (Fig. 9). Given that strawberry PAO5 acts as a negative regulator of ripening by catalyzing the degradation of Spm/Spd (Mo et al., 2020), the stable Put amounts are not derived from Spd/Spm degradation. The downregulation of both *ADC1* and *SAMDC1* expression in the RNAi plants suggests that the stable

Put levels might result from an inhibition of Spd biosynthesis, while the PAO5-mediated degradation functions as a feedback control mechanism. To a large extent, the homeostasis and balance among Put, Spd, and Spm are essential for strawberry vegetative and reproductive growth. Once this balance is disrupted by the abundant FvPAO5 in the *FvCSN5A* RNAi plants, the conversion of Put to Spm is blocked by the undetectable Spd, ultimately leading to abnormal plant development, particularly in the reproductive phase. Integrating our current data and a recent report that the regulation of PA composition, especially the Put/Spm ratio, may be an effective strategy to enhance plant survival and fitness (Navakoudis and Kotzabasis, 2022), we conclude that PA homeostasis is essential for strawberry growth and development in response to environmental cues.

FvCSN5-mediated FvPAO5 degradation coordinates PA and ROS homeostasis to fine-tune strawberry growth

In plants, reactive oxygen species (ROS) function as a double-edged sword, highlighting the importance of ROS homeostasis to accommodate diverse cellular roles and environmental responses (Farooq et al., 2019). Based on the available data and our present findings related to polyamines (PAs), we summarize several key points, including (1) the dual roles of PAs as both ROS scavengers and triggers; (2) the multiple PA components with common and specialized cellular and biological functions, such as putrescine (Put) in photosynthesis, spermine (Spm) in antioxidants, and spermidine (Spd) in both photosynthetic protection and oxidation resistance; (3) the essential role of Spd/Spm in reproductive growth and fitness; and (4) the relationship between increased PAO5 activity and higher H_2O_2 levels. These observations suggest that PAO5 may serve as a hub regulatory checkpoint for the homeostasis and balance of both PA and ROS.

Furthermore, earlier reports indicate that CSN5 is a key component of the COP9 signalosome and participates in various plant processes, including light signaling, circadian rhythm control, cell recycling, and auxin (IAA) signaling (Chamovitz and Segal, 2001; Serino and Deng, 2003). CSN5 functions by mediating the deneddylation of NEDD8 from the cullin subunit of CRL E3 ligases (Schwechheimer and Isono, 2010). This NEDD8-deneddylation is a post-translational modification that affects the activity of cullin-based and non-cullin substrates, and the CSN-mediated deneddylation is required but not essential for CRL-mediated processes (Mergner and Schwechheimer, 2014). Consistent with a previous report, the complete loss of CSN function results in seedling lethality (Stratmann and Gusmaroli, 2012). We now also observed that the inhibition of

FvCSN5A expression not only led to developmental defects in strawberry leaves, flowers, and fruits (Fig. 3-5 and Fig. S2), but also affected PA levels and H_2O_2 production (Fig. 8-9). These results suggest that the post-translational modification of FvPAO5 protein by FvCSN5A contributes to PA homeostasis and the trade-off regulation between these processes.

Although we found that CSN5A interacts with CUL1 as a scaffold, the specific E3 ligase that acts as a receptor for ubiquitylated FvPAO5 remains unknown. The COP9 signalosome (CSN) controls the RUB/NEDD8 modification of several cullin-based E3 ligases, such as SCF^{TIR1}, SCF^{SLY}, SCF^{COI1}, CUL-CDD-RBX1, and CUL-DDB1-COP1-SPA, which are involved in various signal transduction pathways. As the levels of IAA, GA, and JA were affected in *FvCSN5A* RNAi plants (Fig. 8), further investigations are needed to screen for the possible E3 ligases, such as TIR1, SLY, COI1, and COP1, that may directly interact with and regulate FvPAO5.

An integrative model for FvCSN5 and FvPAO5 synergistically regulates the balance among Put, Spd and Spm essential to strawberry vegetative and reproductive growth

To date, we have gained a more comprehensive understanding of the roles of polyamines (PAs) in embryo development, seed germination, seedling growth, reproductive development, and fruit ripening, as well as the relationship between PAs, hydrogen peroxide (H_2O_2), and phytohormone signaling. There is a close relationship between PAs and phytohormones in plant stomatal movement, survival fitness, and fruit ripening (Mo et al., 2020; Liu et al., 2023; Song et al., 2023; Gao et al., 2021, 2024a), with a particular emphasis on the interaction of PAs with ethylene in climacteric tomato fruit ripening and with abscisic acid (ABA) in non-climacteric strawberry fruit ripening (Gao et al., 2021). During the initiation of strawberry fruit ripening, increased ABA suppresses the expression of *FaPAO5* and reduces H_2O_2 production, ultimately facilitating the accumulation of spermine (Spm)/spermidine (Spd) and fruit ripening (Mo et al., 2020). Broadly, PAs, especially Spm, regulate strawberry fruit ripening in an ABA-dominated, indole-3-acetic acid (IAA)-participating, and ethylene-coordinated manner (Guo et al., 2018). Similarly, in response to drought stress, the production of ABA is promoted, which controls PA homeostasis through both reducing putrescine (Put) biosynthesis and accelerating PA metabolism.

Furthermore, IAA is suggested to link to Put-regulating photosynthesis and oxidative phosphorylation, and ABA-regulating sugar and flavonoid metabolism (Gao et al., 2024b). Thus, we consider that PAs, ABA, and IAA weave a core signaling network essential for plant growth and adaptation, primarily through the role of Put in photosynthesis and primary metabolism, which is largely related to vegetative growth, as well as the role of Spd/Spm in secondary metabolism and survival fitness, which is mainly related to reproductive growth. This potentially highlights the equilibrium and trade-off regulation of PA metabolism at the protein level by the feedback control mechanism.

In the present study, we demonstrated that the upregulation of FvPAO5 abundance by inhibiting *FvCSN5A* expression could retard leaf, petal, sepal, and pollen development, as well as fruit ripening, which may be related to the decreased amounts of IAA, ABA, jasmonic acid (JA), Spd/Spm, and sugar, together with the increased levels of salicylic acid (SA), gibberellic acid (GA3), cytokinins (CK), and H_2O_2 (Fig. 8-9). OsPAO5 is a negative regulator for the mesocotyl elongation of rice seedlings, and its knockout mutants facilitate faster seedlings, ultimately increasing grain weight and yield by the higher accumulation of Spm and ethylene, as well as lower accumulation of H_2O_2 and JA (Lv et al., 2021). Also, in Arabidopsis, the loss of AtPAO5 function inhibits the CK-induced shoot meristem formation from lateral root primordia (Kaszler et al., 2023), potentially as a result of the interference of CK and IAA signaling in xylem differentiation (Alabdallah et al., 2017). To a large extent, the synergistic interaction among PAs, reactive oxygen species (ROS), and phytohormones lays a basis for the CSN5-PAO5 module in regulating PA homeostasis and trade-off responsible for strawberry growth transition.

Based on the available data and the present study, we propose a comprehensive model for the FvCSN5A-FvPAO5 coordinate regulation of PA metabolism and H_2O_2 homeostasis, which aligns with plant growth in response to environmental cues in strawberries (Fig. 10). The FvCSN5A-FvCUL1-FvPAO5 model provides novel insights into the integration of the COP9 signalosome into PA metabolism. This is an attractive research field for agricultural foundation and practice in crop yield and quality by the CSN5-integrative signaling, mostly linked to IAA/ABA/JA/ethylene by ROS.

Materials and methods

Plant materials and growth conditions

Octoploid strawberries (*Fragaria* × *ananassa* Duch. cv Benihoppe) grown in a greenhouse under natural sunlight conditions were used for a transient transgenic experiment. Diploid strawberries (*Fragaria vesca*, Rugen) and *Nicotiana benthamiana* were cultured in an artificial climate chamber at 22 ℃, 16h:8h (light:dark).

RNA isolation and RT-qPCR

Total RNA was extracted using the Plant Total RNA Mini-Extraction Kit (Magen, china) and reverse transcription was performed using the Hi fair III 1st Strand cDNA Synthesis Super Mix for qPCR Kit (YEASEN, China). RT-qPCR was performed on a Bio-Rad CFX96 system using the Trans Start Top Green qPCR Super Mix kit (YEASEN, China) with *ACTIN* as an internal control.

Yeast two-hybrid assay

For yeast two-hybrid cDNA library screening, the coding sequence (CDS) of *FvPAO5* was conducted into a pGBKT7 vector. FvPAO5-BD was transformed into yeast gold strain. The yeast strain *FvPAO5* expressed was used to mate with strawberry fruits cDNA library. After 22–24 h, the culture solution was plated on SD/-Ade-His-Leu-Trp medium and incubated for 3–5 days at 30 ℃. The yeast grown on the medium successfully was identified by PCR amplification and sequencing. For one-to-one yeast two-hybrid, the CDS of *FvPAO5* and *FvCUL1* were respectively cloned into pGBKT7, while the CDS of *FvCSN5A* was cloned into the pGADT7 vector. BD-FvPAO5 and AD-FvCSN5A, BD-FvCUL1 and AD-FvCSN5A were cotransformed into yeast cells, respectively, as previously reported (Huang et al., 2024). The transformed yeast cells were cultured on SD/-Leu-Trp medium at 28 ℃ for 3 days. Subsequently, the yeast cells were transferred to SD/-Leu-Trp and SD/-Ade-His-Leu-Trp medium at 28 ℃, and photos were taken 3 days later.

Subcellular localization

The CDS regions of *FvCSN5A* and *FvPAO5* were constructed into the pCAMBIA1300-GFP vector and injected into the leaves of tobacco by Agrobacterium-mediated transient expression. For the locations of the nuclei, *N. benthamiana* leaves were stained with DAPI. CD3-983 was used for the locations of the peroxisome (Nelson et al., 2007). The leaves were observed and photographed with Leica Stellaris 5 laser confocal microscope.

Firefly luciferase complementation assay (FLC**)**

The CDS of *FvPAO5* and *FvCUL1* were cloned into pCAMBIA1300-NLUC, and the CDS of *FvCSN5A* was introduced into pCAMBIA1300-CLUC. The constructs were cotransfected into *Nicotiana benthamiana* leaves. The luminescence signals were recorded with a cold CCD camera 3 days later.

Bimolecular fluorescence complementation (BiFC) assay

The CDS of *FvPAO5* were cloned into pSPYNE173, and the CDS of *FvCSN5A* was cloned into pSPYCE. The constructs were cotransfected into *Nicotiana benthamiana* leaves. GFP signals were detected after 3 days using laser confocal microscopy (Leica Stellaris 5).

Co-Immunoprecipitation (CoIP) assay

pSP1300:FvCSN5A-MYC and pSP1300:FvPAO5-GFP constructs were cotransfected into *Nicotiana benthamiana* leaves. Leaves were collected after 2 days, and total proteins were extracted with protein lysis buffer (100 mM Tris-HCl, pH 7.5, 50 mM NaCl, 5 mM EDTA, 1% Tritonx-100, 1% Tween- 20 and 1% NP-40) to extract total protein. Total proteins were incubated with MYC beads for 3 h. The target proteins were detected with anti-MYC antibody and anti-GFP antibody.

GST pull-down assay

The CDS of *FvPAO5* was cloned into pGEX4T-1 (GST-tagged) and the CDS of *FvCSN5A* was cloned into pET-30a (His-tagged). Proteins were expressed in BL21 *Escherichia coli*. Recombinant FvPAO5-GST was purified and incubated with 20 μL glutathione Sepharose 4B in pull-down buffer (20 mM Tris–HCl, pH 7.5, 150 mM NaCl, 1 mM β-mercaptoethanol, 3 mM EDTA, pH 8.0, and 1% NP-40) for 1 h, and then FvCSN5A-His was added and incubated for 1 h. The results were detected by immunoblotting using anti-His and anti-GST antibodies.

Cell-free protein degradation and in vivo ubiquitination assay

The leaves of three-month-old 'Ruegen' strawberry seedlings were harvested to extract the total plant protein with protein lysis buffer (100 mM HEPS, 1 mM EDTA, pH 7.8, 10% glycerol, 1% Tritonx-100, 1 mM DTT, 1 mM PMSF, 1% Cocktail). The purified FvPAO5-GST protein and total strawberry protein were mixed with DMSO or 50 μM MG132, respectively, and the samples were incubated at 20 ℃ for different times. Anti-GST and Anti-ACTIN antibodies were used for immunoblotting detection.

In the *in vivo* ubiquitination assay, three-month-old WT and *FvCSN5A* RNAi transgenic seedlings were cultured in liquid MS medium at 25 ℃ for 5 h with or with DMSO or 50 μM MG132 (stock

solution prepared with 0.5% DMSO) and 100 μM CHX (cycloheximide, an inhibitor of protein synthesis). The total proteins were extracted as described above, and the total protein was incubated with ubiquitin-trap bead p62-agarose at 4 ℃ for 4 h. The ubiquitination signal was detected by Anti-PAO5 antibody, while the Input sample was detected by Anti-ACTIN antibody.

RNAi vector construction and plant transformation

The 300 bp *FvCSN5A* fragment was constructed into pK7GWIWG2 (II) vector for RNAi, and was transformed into *Agrobacterium tumefaciens* strain GV3101. *Agrobacterium tumefaciens* cultures were incubated at 28 ℃, with a final OD_{600} value of 0.5, and then infiltrated into the diploid strawberry "Ruegen" by the leaf disc method (Li et al., 2018). The transgenic strawberry lines were identified by fluorescence screening and RT-qPCR.

Strawberry fruit transient transgene

The CDS of *FaCSN5A* was constructed into pCAMBIA1300-GFP vector to obtain the overexpression vector. Agrobacterium transformed *FaCSN5A* OE, control and *FaCSN5A* RNAi were incubated at 28 ℃ with a final OD600 value of 0.5, and de-greening stage fruits were selected to inject. Ten fruits were used in each treatment. Photos were taken every day to record the phenotypes. Samples were harvested and achenes were removed 5 days after injection. The injection site was cut, and the injected parts were frozen in liquid nitrogen and stored at -80 ℃.

In vitro germination of pollen grains

The anthers from freshly opened WT and *FvCSN5A* RNAi transgenic flowers were harvested and pollen grains were released and incubated with pollen grain germination medium (10% sucrose, 0.002% boric acid, and 0.5% agar) at 22 ℃ for 5 h. The pollen grains were taken to slides and photographed using a microscope.

Alexandria stain

The anthers from freshly opened WT and *FvCSN5A* RNAi transgenic flowers were harvested and Alexander's staining solution (Coolabor, China.) was placed on the anthers. The anthers were gently peeled off with tweezers, and the pollen grains were released into the staining solution for 6 h. The pollen grains were observed and photographed under a microscope.

Determination of anthocyanin content

The determination of anthocyanin content was carried out as the procedure described in the plant anthocyanin content detection kit (Solarbio, China). 0.1 g strawberry sample powder was used in this experiment.

Determination of soluble sugar content

Soluble sugar content was determined by the previous method (Huang et al., 2019). 0.5 g strawberry fruit powder was dissolved in 80% ethanol at 80 ℃ for 30 min and repeated three times. After centrifugation, the supernatant was boiled to dryness and dissolved in ultrapure water. The solution was filtered using LC-18 SPE and determined by HPLC. D-(+) glucose, D-(-) fructose and sucrose were used as standards.

Determination of polyamine and phytohormone content

For determination of polyamine, 0.5 g strawberry leaf powder was incubated with 5% perchloric acid at 4 ℃ for 1 h. Centrifugation was carried out at 4℃ for 30 min at 12,000 g. The extracted supernatant was mixed with benzoyl chloride and then assayed for PA using an HPLC system.

To detect the content of phytohormone, 0.5 g strawberry leaf powder was weighed, 8 mL of methanol-formic acid solution (99:1, v/v) was added as extractant, and the extract was passed through a 0.45 μm organic filter membrane.

Detection and measurement of H_2O_2

For DAB staining, strawberry leaves and anthers were incubated with DAB working staining solution (DAB color development kit, Solarbio, China) at room temperature for 4 h. Strawberry leaves and anthers were decolorized using 95% ethanol at 80 ℃ for 20 min. The DAB samples were immersed in the preservation solution for 30 min. Pollen grains and leaves were photographed using a microscope, respectively.

For fluorescent detection of ROS using DCFH-DA, strawberry leaves and anthers were incubated with 5 μM DCFH-DA working staining solution (Solarbio, China) at room temperature for 10 min, and washed twice in PBS. Pollen grains and leaves were observed and photographed with a Leica Stellaris 5 laser confocal microscope.

For measurement of H_2O_2 following the method reported by (Gay and Gebicki, 2003), 0.2 g strawberry leaf powder was incubated with pre-cooled acetone extraction buffer, and then extractant [(CCL4: CHCL3=3:1 (V:V)] and distilled water were added. The solution was centrifuged at 5000

r/min for 10 min, and the upper aqueous phase was taken to add the working reagent. After 30 minutes 30 ℃ water bath, the content of H_2O_2 was determined at A560 nm.

Statistical analysis

Statistical analysis was performed using SigmaPlot version 12.0 (Systat software, USA). Data are reported as the mean ± SE. Asterisks indicate significant differences between each treatment, assessed by Student's t-test. *P < 0.05; **, P < 0.01. Different letters indicate statistically significant differences at P<0.05 as determined by Student's t-test.

Author contributions

GJX and GF conceived the study and managed the projects; GJH and HY performed the experiments and performed data analysis. HY, SYY, GJX and GF wrote and revised the article.

Data availability

The data underlying this article are available in the article and in its online supplementary material.

Acknowledgments

This work was supported by the National Natural Science Foundation of China (32030100; 32072516; 32272648).

Competing interests

The authors declare that no competing interests exist.

References

Alabdallah O, Ahou A, Mancuso N, Pompili V, Macone A, Pashkoulov D, Stano P, Cona A, Angelini R, Tavladoraki P. The Arabidopsis polyamine oxidase/dehydrogenase 5 interferes with cytokinin and auxin signaling pathways to control xylem differentiation. Journal of Experimental Botany, 2017, 68(5): 997-1012.

Aloisi I, Piccini C, Cai G, Del Duca S. Male Fertility under Environmental Stress: Do Polyamines Act as Pollen Tube Growth Protectants?. International Journal of Molecular Sciences, 2022, 23(3): 1874.

Barry M, Früh K. Viral modulators of cullin RING ubiquitin ligases: culling the host defense. Science's STKE, 2006, 2006(335): pe21.

Blázquez MA. Polyamines: Their Role in Plant Development and Stress. Annual Review of Plant Biology, 2024, 75. Available from: https://doi.org/10.1146/annurev-arplant-070623-110056

Chamovitz DA, Segal D. JAB1/CSN5 and the COP9 signalosome. A complex situation. EMBO Reports, 2001, 2(2): 96-101.

Cope GA, Deshaies RJ. COP9 signalosome: A multifunctional regulator of SCF and other cullin-based ubiquitin ligases. Cell, 2003, 114: 663–671.

Dong J, Li Y, Cheng S, Li X, Wei N. COP9 signalosome-mediated deneddylation of CULLIN1 is necessary for SCF^{EBF1} assembly in *Arabidopsis thaliana*. Cell reports, 2024, 43(1): 113638.

Farooq MA, Niazi AK, Akhtar J, Saifullah, Farooq M, Souri Z, Karimi N, Rengel Z. Acquiring control: The evolution of ROS-Induced oxidative stress and redox signaling pathways in plant stress responses. Plant Physiology and Biochemistry. 2019, 141: 353-369.

Fischer ES, Scrima A, Böhm K, Matsumoto S, Lingaraju GM, Faty M, Yasuda T, Cavadini S, Wakasugi M, Hanaoka F, Iwai S, Gut H, Sugasawa K, Thomä NH. The molecular basis of CRL4DDB2/CSA ubiquitin ligase architecture, targeting, and activation. Cell, 2011, 147: 1030-1039.

Fortes AM, Agudelo-Romero P, Pimentel D, Alkan N. Transcriptional modulation of polyamine metabolism in fruit species under abiotic and biotic stress. Frontiers in Plant Science, 2019, 10: 816.

Furumoto T, Yamaoka S, Kohchi T, Motose H, Takahashi T. Thermospermine is an evolutionarily ancestral phytohormone required for organ development and stress responses in Marchantia polymorpha. Plant & Cell Physiology, 2024, 65(3): 460-471.

Gao F, Mei XR, Li YZ, Guo JX, Shen YY. Update on the roles of polyamines in fleshy fruit ripening, senescence, and quality. Frontiers in Plant Science, 2021, 12: 610313.

Gao F, Li JY, Li WJ, Shi S, Song SH, Shen YY, Guo JX. Abscisic acid and polyamines coordinately regulate strawberry drought responses. Plant Stress, 2024a, 11: 100387.

Gao F, Guo J, Shen Y. Advances from chlorophyll biosynthesis to photosynthetic adaptation, evolution and signaling. Plant Stress, 2024b, 12: 100470.

Gay CA, Gebicki JM. Measurement of protein and lipid hydroperoxides in biological systems by the ferric-xylenol orange method. Anal Biochemistry, 2003, 315(1):29-35.

Guo J, Wang S, Yu X, Dong R, Li Y, Mei X, Shen Y. Polyamines regulate strawberry fruit ripening by abscisic Acid, auxin, and ethylene. Plant Physiology. 2018, 177(1): 339-351.

Gupta K, Sengupta A, Chakraborty M, Gupta B. Hydrogen peroxide and polyamines act as double edged swords in plant abiotic stress responses. Frontiers in Plant Science, 2016, 7: 1343.

Gusmaroli G, Feng S, Deng XW. The Arabidopsis CSN5A and CSN5B subunits are present in distinct COP9 signalosome complexes, and mutations in their JAMM domains exhibit differential dominant negative effects on development. The Plant Cell, 2004, 16: 2984-3001.

Hotton SK, Callis J. Regulation of cullin RING ligases. Annual Review of Plant Biology, 2008, 59: 467-489.

Huang F, Sun M, Yao Z, Zhou J, Bai Q, Chen X, Huang Y, Shen Y. Protein kinase FaSnRK2.6 phosphorylates transcription factor FabHLH3 to regulate anthocyanin homeostasis during strawberry fruit ripening. Journal of Experimental Botany, 2024, 29:erae250.

Huang X, Hetfeld BK, Seifert U, Kahne T, Kloetzel PM, Naumann M, Bech-Otschir D, Dubiel W. Consequences of COP9 signalosome and 26S proteasome interaction. The FEBS Journal, 2005, 272: 3909-3917.

Huang Y, Xu PH, Hou BZ, Shen YY. Strawberry tonoplast transporter, FaVPT1, controls phosphate accumulation and fruit quality. Plant Cell & Environment, 2019, 42(9): 2715-2729.

Jasso-Robles FI, Gonzalez ME, Pieckenstain FL, Ramírez-García JM, Guerrero-González ML, Jiménez-Bremont JF, Rodríguez-Kessler M. Decrease of Arabidopsis PAO activity entails increased RBOH activity, ROS content and altered responses to *Pseudomonas*. Plant Science, 2020, 292: 110372.

Jin D, Li B, Deng XW, Wei N. Plant COP9 signalosome subunit 5, CSN5. Plant Science, 2014, 224: 54-61.

Kaszler N, Benkő P, Molnár Á, Zámbori A, Fehér A, Gémes K. Absence of Arabidopsis polyamine oxidase 5 influences the cytokinin-induced shoot meristem formation from lateral root primordia. Plants, 2023, 12(3): 454.

Kwok SF, Solano R, Tsuge T, Chamovitz DA, Ecker JR, Matsui M, Deng XW. Arabidopsis homologs of a c-Jun coactivator are present both in monomeric form and in the COP9 complex, and their abundance is differentially affected by the pleiotropic cop/det/fus mutations. The Plant Cell, 1998, 10: 1779-1790.

Li W, Zhang J, Sun H, Wang S, Chen K, Liu Y, Li H, Ma Y, Zhang Z. FveRGA1, encoding a DELLA protein, negatively regulates runner production in Fragaria vesca. Planta, 2018, 247(4): 941-951.

Liao X, Li M, Liu B, Yan M, Yu X, Zi H, Liu R, Yamamuro C. Interlinked regulatory loops of ABA catabolism and biosynthesis coordinate fruit growth and ripening in woodland strawberry. Proceedings of the National Academy of Sciences of the United States of America, 2018, 115(49): E11542-E11550.

Liu X, Reitsma JM, Mamrosh JL, Zhang Y, Straube R, Deshaies RJ. Cand1-mediated adaptive exchange mechanism enables variation in F-box protein expression. Molecular Cell, 2018, 69(5): 773-786.

Liu XD, Zeng YY, Zhang XY, Tian XQ, Hasan MM, Yao GQ, Fang XW. Polyamines inhibit abscisic acid-induced stomatal closure by scavenging hydrogen peroxide. Physiologia Plantarum, 2023, 175(2): e13903.

Lingaraju GM, Bunker RD, Cavadini S, Hess D, Hassiepen U, Renatus M, Fischer ES, Thoma NH. Crystal structure of the human COP9 signalosome. Nature, 2014, 512: 161-165.

Lv Y, Shao G, Jiao G, Sheng Z, Xie L, Hu S, Tang S, Wei X, Hu P. Targeted mutagenesis of POLYAMINE OXIDASE 5 that negatively regulates mesocotyl elongation enables the generation of direct-seeding rice with improved grain yield. Molecular plant, 2021, 14(2): 344-351.

Lyapina S, Cope G, Shevchenko A, Serino G, Tsuge T, Zhou C, Wolf DA, Wei N, Shevchenko A, Deshaies RJ. Promotion of NEDD-CUL1 conjugate cleavage by COP9 signalosome. Science, 2001, 292: 1382-1385.

Mayor-Ruiz C, Jaeger MG, Bauer S, Brand M, Sin C, Hanzl A, Mueller AC, Menche J, Winter GE. Plasticity of the cullin-RING ligase repertoire shapes sensitivity to ligand-induced protein degradation. Molecular Cell, 2019, 75: 849-858.

Mergner J, Schwechheimer C. The NEDD8 modification pathway in plants. Frontiers in Plant Science. 2014, 5:103.

Mo AW, Xu T, Bai Q, Shen YY, Gao F, Guo JX. FaPAO5 regulates Spm/Spd levels as a signaling during strawberry fruit ripening. Plant Direct, 2020, 4(5): e00217.

Nandy S, Das T, Tudu CK, Mishra T, Ghorai M, Gadekar VS, Anand U, Kumar M, Behl T, Shaikh NK, Jha NK, Shekhawat MS, Pandey DK, Dwivedi P, Radha, Dey A. Unravelling the multi-faceted regulatory role of polyamines in plant biotechnology, transgenics and secondary metabolomics. Applied Microbiology and

Biotechnology, 2022, 106(3): 905-929.
Napieraj N, Janicka M, Reda M. Interactions of polyamines and phytohormones in plant response to abiotic stress. Plants, 2023, 12(5): 1159.
Navakoudis E, Kotzabasis K. Polyamines: A bioenergetic smart switch for plant protection and development. Journal of Plant Physiology, 2022, 270: 153618.
Nelson BK, Cai X, Nebenführ A. A multicolored set of in vivo organelle markers for co-localization studies in Arabidopsis and other plants. The Plant Journal, 2007, 51(6): 1126-1136.
Pottosin I, Velarde-Buendía AM, Bose J, Zepeda-Jazo I, Shabala S, Dobrovinskaya O. Cross-talk between reactive oxygen species and polyamines in regulation of ion transport across the plasma membrane: implications for plant adaptive responses. Journal of Experimental Botany, 2014, 65(5): 1271-1283.
Qin N, Xu D, Li J, Deng XW. COP9 signalosome: Discovery, conservation, activity, and function. Journal of integrative plant biology, 2020, 62(1): 90-103.
Reitsma JM, Liu X, Reichermeier KM, Moradian A, Sweredoski MJ, Hess S, Deshaies RJ. Composition and regulation of the cellular repertoire of SCF ubiquitin ligases. Cell, 2017, 171(6): 1326-1339.
Russell DH. The roles of polyamines, putrescine, spermidine and spermine in normal and malignant tissues. Life Science, 1973, 13: 1635–1647.
Schwechheimer C, Serino G, Deng XW. Interactions of the COP9 signalosome with the E3 ubiquitin ligase SCFTIR1 in mediating auxin response. Science, 2001, 292: 1379-1382.
Schwechheimer C, Isono E. The COP9 signalosome and its role in plant development. European Journal of Cell Biology. 2010, 89(2): 157-162.
Serino G, Deng XW. The COP9 signalosome: regulating plant development through the control of proteolysis. Annual Review of Plant Biology, 2003, 54(1):165-182.
Shang Y, Wang K, Sun S, Zhou J, Yu JQ. COP9 Signalosome CSN4 and CSN5 subunits are involved in jasmonate-dependent defense against root-knot nematode in tomato. Frontier in Plant Science, 2019, 10: 1223.
Shen ZF, Li L, Wang JY, Liao J, Zhang YR, Zhu XM, Wang ZH, Lu JP, Liu XH, Lin FC. CSN5 inhibits autophagy by regulating the ubiquitination of Atg6 and Tor to mediate the pathogenicity of *Magnaporthe oryzae*. Cell Communication and Signaling, 2024, 22(1): 222.
Siddappa S, Marathe GK. What we know about plant arginases?. Plant Physiology and Biochemistry, 2020, 156: 600-610.
Song J, Sun P, Kong W, Xie Z, Li C, Liu JH. SnRK2.4-mediated phosphorylation of ABF2 regulates ARGININE DECARBOXYLASE expression and putrescine accumulation under drought stress. New Phytologist, 2023, 238(1): 216-236.
Stratmann JW, Gusmaroli G. Many jobs for one good cop - the COP9 signalosome guard development and defense. Plant Science, 2012, 185-186: 50-64.
Verma R, Aravind L, Oania R, McDonald WH, Yates JR, Koonin EV, Deshaies RJ. Role of Rpn11 metalloprotease in deubiquitination and degradation by the 26S proteasome. Science, 2002, 298: 611–615
Wang W, Paschalidis K, Feng JC, Song J, Liu JH. Polyamine catabolism in plants: A universal process with diverse functions. Frontiers in Plant Science, 2019, 10: 561.

Wei N, Deng XW. The COP9 signalosome. Annual Review of Cell and Developmental Biology, 2003, 19(1): 261-286.

Yu Z, Jia DY, Liu TB. Polyamine oxidases play various roles in plant development and abiotic stress tolerance. Plants, 2019, 8(6): 184.

Zhan ZN, Wang N, Chen ZM, Zhang YX, Geng KQ, Li DM, Wang ZP. Effects of water stress on endogenous hormones and free polyamines in different tissues of grapevines (*Vitis vinifera* L. cv. 'Merlot'). Functional Plant Biology, 2023, 50(12): 993-1009.

Zhao JQ, Wang XF, Pan XB, Jiang QQ, Xi ZM. Exogenous putrescine alleviates drought stress by altering reactive oxygen species scavenging and biosynthesis of polyamines in the seedlings of Cabernet Sauvignon. Frontiers in Plant Science, 2021, 12: 767992.

Zhong M, Yue L, Liu W, Qin H, Lei B, Huang R, Yang X, Kang Y. Genome-wide identification and characterization of the polyamine uptake transporter (Put) gene family in tomatoes and the role of Put2 in response to salt stress. Antioxidants, 2023, 12(2): 228.

Figure legend

Fig.1 FvCSN5A interacted with FvPAO5 *in vitro* and *in vivo*.

A. FvCSN5A interacted with FvPAO5 in yeast two-hybrid assay. SD-LW: synthetic dropout medium without Leu and Trp; SD-LWHA: synthetic dropout medium without Leu, Trp, His, and Ade.

B. *In vitro* pull-down assay showing that FvCSN5A interacts with FvPAO5. Recombinant GST or FvPAO5-GST bounded to Glutathione Sepharose beads was incubated with recombinant FvCSN5A-His protein. Input and elution proteins immunoblotted with Anti-His and Anti-GST antibody, respectively.

C. Firefly luciferase complementation (FLC) assays were performed to verify the interaction between FvCSN5A and FvPAO5. The CDS of *FvCSN5A* was constructed into pCAMBIA1300-CLUC vector, and the CDS of *FvPAO5* was constructed into pCAMBIA1300-NLUC vector.

D. *In vivo* Co-Immunoprecipitation (CoIP) assay showing that FvCSN5A interacts with FvPAO5. FvCSN5A-MYC protein bounded to MYC beads was incubated with GFP or FvPAO5-GFP and immunoblotted with Anti-GFP antibody and Anti-MYC antibody, respectively.

E. FvCSN5A and FvPAO5 interacted in bimolecular fluorescence complementation (BiFC) assay. FvCSN5A was fused to the C terminus of YFP and FvPAO5 to the N terminus of YFP. The encoding constructs were co-infiltrated into *N. benthamiana* leaves. Bars, 50 μm.

Fig. 2 *FvCSN5A* expression pattern and subcellular localization.

A. The transcript level of *FvCSN5A* in different tissues of diploid strawberry (*F. vesca*, 'Ruegen'). Different letters indicate statistically significant differences at P<0.05 as determined by Student's t-test.

B. *FvCSN5A* transcript levels in fruit receptacles at different developmental stages of diploid strawberry (*F. vesca*, 'Ruegen'). SG, small green fruit stage; Wt, white fruit stage; IR, initial red fruit stage; PR, partial red fruit stage; FR, full ripening fruit stage. Relative expression values were relative to receptacles at the SG stage in all cases, which was assigned an arbitrary value equal to one. Different letters indicate statistically significant differences at P<0.05 as determined by Student's t-test.

C. Subcellular localization of FvCSN5A-GFP fusions in transiently transformed *N. benthamiana* leaves. All experiments were assayed 48 h after infiltration. Bars, 20 μm. For the locations of the nuclei, *N. benthamiana* leaves were stained with DAPI. Px-rk/CD3-983 was a marker for the locations of the peroxisome.

Fig. 3 Phenotypes of the *FvCSN5A* RNAi transgenic plants.

A. Visualization of DsRed accumulation in *FvCSN5A* RNAi plants (right). Bars, 1 cm.

B. Relative expression levels of *FvCSN5A* was determined by RT-qPCR. Statistical significance was determined by Student's t-test. *P < 0.05, **P < 0.01.

C. The photo of wild-type (WT, *F. vesca*, 'Ruegen') and *FvCSN5A* RNAi transgenic plants in soil. Bars, 1 cm.

D. One compound leaf of WT and *FvCSN5A* RNAi transgenic plants. Bars, 1 cm.

E. The flowers of WT and *FvCSN5A* RNAi transgenic plants. Bars, 1 cm.

F. The sepals of WT and *FvCSN5A* RNAi transgenic plants. Bars, 1 cm.

G. Leaf shape index of WT and *FvCSN5A* RNAi transgenic plants.

H. Numbers of the serrations of WT and *FvCSN5A* RNAi transgenic plants.

I. Depth of the serrations of WT and *FvCSN5A* RNAi transgenic plants. **, P < 0.01; Student's t-test.

J. The percentages of different types of sepals in WT and *FvCSN5A* RNAi transgenic plants. n = 36.

K. The percentages of different types of petals in WT and *FvCSN5A* RNAi transgenic plants. n = 36.

Fig. 4 Pistils and anthers phenotypes of the *FvCSN5A* RNAi transgenic plants.

A-B. The images of pistil (A) and anther (B) of WT and *FvCSN5A* RNAi transgenic plants.

C-D. Numbers of pistil (C) and anther (D) of WT and *FvCSN5A* RNAi transgenic plants. **, $P < 0.01$; Student's t-test.

E. The images showing Alexander's staining of pollen grains from WT and *FvCSN5A* RNAi transgenic plants. The red-stained pollen grains are viable and fertile.

F. The images showing pollen tubes of WT and *FvCSN5A* RNAi transgenic plants germination in vitro. Bars, 100 μm.

G. The percentages of Alexander's staining of pollen grains from WT and *FvCSN5A* RNAi transgenic plants. **, $P < 0.01$; Student's t-test.

H. The percentages of WT and *FvCSN5A* RNAi pollen tubes germinated *in vitro*. *$P < 0.05$; **, $P < 0.01$; Student's t-test.

I. The length of WT and *FvCSN5A* RNAi pollen tubes germinated *in vitro*. **, $P < 0.01$; Student's t-test.

J. The diameter length of pollen grains from WT and *FvCSN5A* RNAi transgenic plants. **, $P < 0.01$; Student's t-test.

Fig. 5 Fruit ripening changes in *FvCSN5A* transgenic fruits.

A. Photos were taken at 15, 17, 19, 21, 23, and 25 days after pollination respectively to record the fruit phenotype.

B-E. The anthocyanin content (B), firmness (C) fresh weight (D), and soluble sugar content (E) of *FvCSN5A* transgenic and WT fruits. Bars are means SEs of three independent experiments (Student's t-test; **$P < 0.01$).

F. RT-qPCR was used to analyze the genes' expression in *FvCSN5A* transgenic and WT fruits, and three biological replicates were tested for all samples using the Actin gene from strawberry as an internal control. The relative expression levels were calculated using the $2^{-\triangle\triangle Ct}$ method. FvCSN5A: COP9 Signalosome5; FvPG: polygalacturonase; FvCEL: cellulose; FvCHS: chalcone synthase; FvANS: anthocyanidin synthase; FvSUT1: sucrose transporter1; FvSS: sucrose synthase. FvADC1:

arginine decarboxylase1; FvSAMDC1: S-adenosyl-methionine decarboxylase1; FvSPDS: spermidine synthase; FvSPMS: spermine synthase; FvPAO5: polyamine oxidase5. *P < 0.05; **, P < 0.01; Student's t-test.

Fig. 6 The ubiquitination degradation of FvPAO5 is dependent on FvCSN5A.

A. Cell free FvPAO5 protein degradation. Total protein was extracted from strawberry leaves and incubated with FvPAO5-GST protein for 0.5, and 1 h with MG132 treatment or DMSO treatment as a control. FvPAO5-GST protein and Total plant protein were detected by Anti-GST and Anti-ACTIN, respectively.

B. FvPAO5 and FvCSN5A protein aboundance detection in *FvCSN5A* RNAi and WT plants. FvPAO5 and FvCSN5A were detected by Anti-FvPAO5 and Anti- FvCSN5A, respectively.

C. *In vivo* FvPAO5 polyubiquitination in *FvCSN5A* RNAi and WT plants. Three-month-old seedlings were transferred to MS medium supplemented with or without 50 μM MG132 for 5 h and then harvested for protein extraction. Each total protein was incubated with P62-agarose to obtain ubiquitinated proteins. Polyubiquitinated FvPAO5 was detected with an anti- FvPAO5 antibody. The accumulation of ACTIN in the total protein was tested as a control.

Fig. 7 FvCUL1 interacted with FvCSN5A *in vitro* and *in vivo*.

A. The transcript level of *FvCUL1* in different tissues of strawberry. Different letters indicate statistically significant differences at P<0.05 as determined by Student's t-test.

B. *FvCUL1* transcript levels in fruit receptacles at different developmental stages of diploid strawberry. Different letters indicate statistically significant differences at P<0.05 as determined by Student's t-test.

C. FvCUL1 interacted with FvCSN5A in FLC assay. The CDS of *FvCSN5A* was constructed into pCAMBIA1300-CLUC vector, and the CDS of *FvCUL1* was constructed into pCAMBIA1300-NLUC vector.

D. FvCUL1 interacted with FvCSN5A in yeast two-hybrid assay. SD-LW: synthetic dropout medium without Leu and Trp; SD-LWHA: synthetic dropout medium without Leu, Trp, His, and Ade.

E. Detection of FvCUL1 protein in *FvCSN5A* RNAi and WT plants using antibody Anti-CUL1.

NED- FvCUL1: FvCUL1 with neddylation; deNED- FvCUL1: FvCUL1 without neddylation.

Fig. 8 Polyamine and phytohormone content in *FvCSN5A* RNAi transgenic plants

A-C: Spm (A), Spd (B), and Put (C) content in WT and *FvCSN5A* RNAi transgenic leaves.

D-L. Phytohormone IAA, ABA, JA, GA3, SA, tZR, DHZR, HZ-2 and tZ content in WT and *FvCSN5A* RNAi transgenic leaves. *P < 0.05; **, P < 0.01; Student's t-test.

Fig. 9 Detection of ROS accumulation in *FvCSN5A* RNAi transgenic plants

A. DAB dye of pollen grains from *FvCSN5A* RNAi and WT plants. Bars, 50 μm.

B. DAB dye of one compound leaf from *FvCSN5A* RNAi and WT plants. Bars, 1cm.

C. ROS signal of pollen grains determinated by DCFH-DA. Bars, 20 μm.

D. ROS signal of leaf determinated by DCFH-DA. Bars, 50 μm.

E. The content of H_2O_2 in *FvCSN5A* RNAi transgenic plants and WT.

Fig. 10 proposed working model

An equilibrium regulation for the composition and content of Put, Spd and Spm, is programmed by PA biosynthesis and degradation: Put-related key enzymes is ADC1; Spd/Spm-related key enzymes include SAMDC1, SPDS, and SPDM for biosynthesis and PAO5 for degradation. In response to environments, the two equilibria from Put/Spd/Spm metabolism to vegetative/reproductive growth are fine-tuned at transcripts, translation and post-translation for plant better growth and breeding. The CSN5A interacting with CUL1 miediates degradation of PAO5, not only rapidly controling PA balance, but also H_2O_2 production, which could be integrated into various hormones. Finally, PAs, ROS and hormones synergistically regulates strawberry development and adaptation.

CSN5A is essential for the deneddylation of CUL1, which may affect the protein stability of CUL1 and SCF E3 ubiquitin ligase activity. CUL1 protein level in the *FvCSN5A* RNAi markedly decreases, and PAO5 increases. These changes lead to the significant decrease of PA, Auxin, ABA, JA content, and excessive accumulation of H_2O_2. The homeostasis disruption in *FvCSN5A* RNAi plants may be responsible for the growth defects, slow fruit ripening and poor fertility phenotype.

Supplemental files

Supplemental Fig. 1 *FvCSN5A* RNAi transgenic callus screening.

The red calluses were *FvCSN5A* RNAi successful transgenic callus, which were named *FvCSN5A* RNAi-1 and *FvCSN5A* RNAi-2.

Supplemental Fig. 2 Reciprocal crosses between WT and *FvCSN5A* RNAi -2 plant

Supplemental Fig. 3 Observation of fruit development process of *FvCSN5A* RNAi-2 transgenic plant.

Photos were taken at 15, 17, 19, 21, 23, and 25 days after pollination respectively to record the fruit phenotype.

Supplemental Fig. 4 Manipulation of *FaCSN5A* expression affected physiological parameters and transcript levels of ripening-related genes.

A. Phenotypes of *FaCSN5A* OE and *FaCSN5A* RNAi strawberry fruits. Agrobacterium GV3101 strains containing RNAi or overexpression *FaCSN5A* recombinant plasmids were injected into DG fruits attached to the plant. The fruit phenotype was recorded at 0, 2, 3, 4, and 5 days after injection. Bars, 1 cm.

B. Analysis of *FaCSN5A* transcript levels in *FaCSN5A* OE and *FaCSN5A* RNAi fruits compared with the control. *$P < 0.05$; **, $P < 0.01$; Student's t-test.

C-E. The anthocyanin content (C), soluble sugar content (D), and firmness (E) of *FaCSN5A* OE and *FaCSN5A* RNAi strawberry fruits. **, $P < 0.01$; Student's t-test.

F. RT-qPCR was used to analyze the genes' expression in *FaCSN5A* OE and *FaCSN5A* RNAi fruits. Relative expression levels were calculated using the 2-△△Ct method. FaPG: polygalacturonase; FaCEL: cellulose; FaCHS: chalcone synthase; FaANS: anthocyanidin synthase; FaSUT1: sucrose transporter1; FaSS: sucrose synthase. FaADC1: arginine decarboxylase1; FaSAMDC1: S-adenosyl-methionine decarboxylase1; FaSPDS1: spermidine synthase1; FaSPMS: spermine synthase; FaPAO5: polyamine oxidase5. *$P < 0.05$; **, $P < 0.01$; Student's t-test.

Supplemental Table 1 The list of primers used in the experiments.

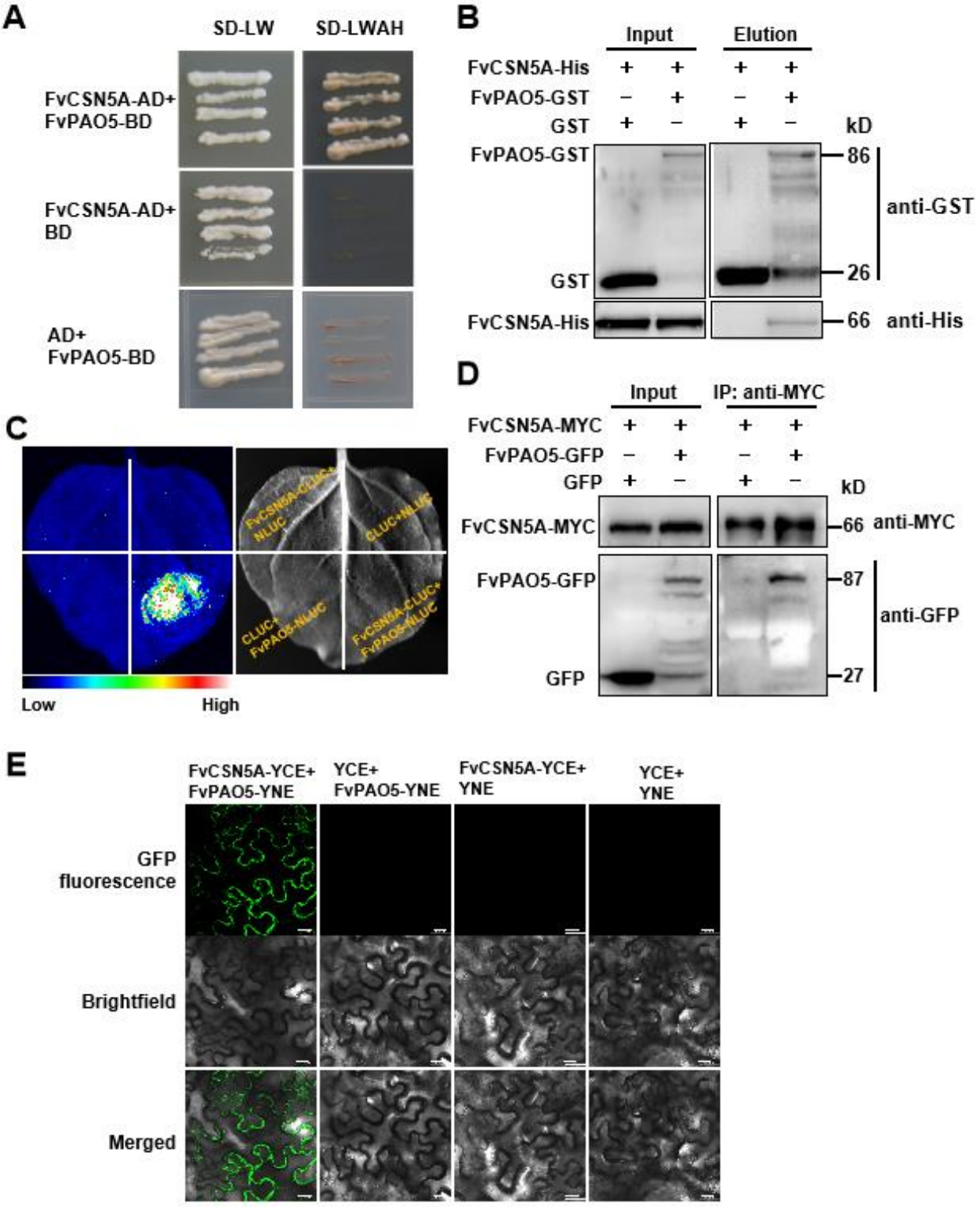

Fig.1 FvCSN5A interacted with FvPAO5 in *vitro* and in *vivo*.

A. FvCSN5A interacted with FvPAO5 in yeast two-hybrid assay. SD-LW: synthetic dropout medium without Leu and Trp; SD-LWHA: synthetic dropout medium without Leu, Trp, His, and Ade.

B. In *vitro* pull-down assay showing that FvCSN5A interacts with FvPAO5. Recombinant GST or FvPAO5-GST bounded to Glutathione Sepharose beads was incubated with recombinant FvCSN5A-His protein. Input and elution

proteins immunoblotted with Anti-His and Anti-GST antibody, respectively.

C. Firefly luciferase complementation assays were performed to verify the interaction between FvCSN5A and FvPAO5. The CDS of *FvCSN5A* was constructed into pCAMBIA1300-CLUC vector, and the CDS of FvPAO5 was constructed into pCAMBIA1300-NLUC vector.

D. In *vivo* Co-Immunoprecipitation (CoIP) assay showing that FvCSN5A interacts with FvPAO5. FvCSN5A-MYC protein bounded to MYC beads was incubated with GFP or FvPAO5-GFP and immunoblotted with Anti-GFP antibody and Anti-MYC antibody, respectively.

E. FvCSN5A and FvPAO5 interacted in bimolecular fluorescence complementation (BiFC) assay. FvCSN5A was fused to the C terminus of YFP and FvPAO5 to the N terminus of YFP. The encoding constructs were co-infiltrated into *N. benthamiana* leaves. Bars, 20 μm.

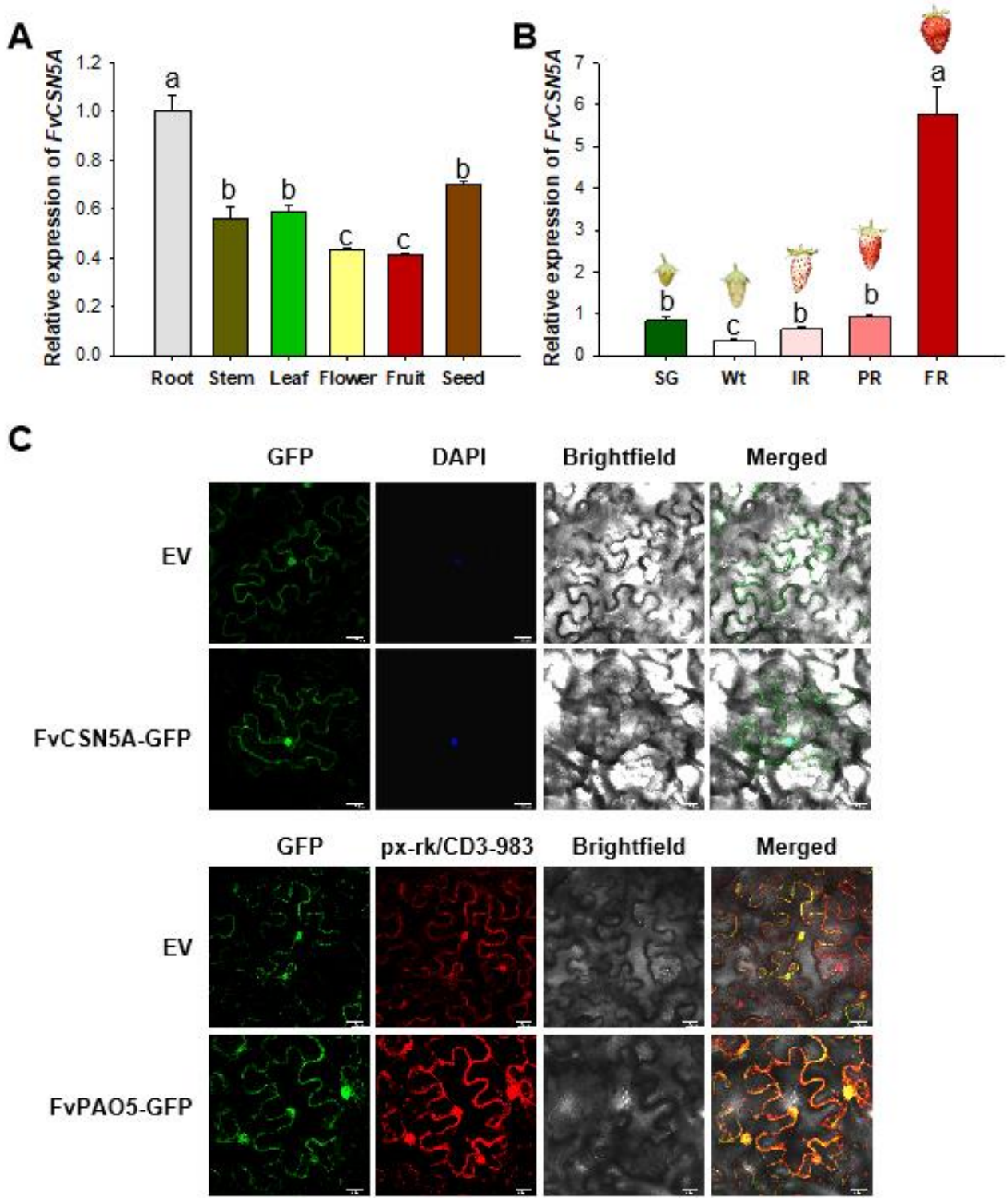

Fig. 2 FvCSN5A expression pattern and subcellular localization.

A. The transcript level of *FvCSN5A* in different tissues of diploid strawberry (*F. vesca*, 'Ruegen'). Different letters indicate statistically significant differences at P<0.05 as determined by Student's t-test.

B. *FvCSN5A* transcript levels in fruit receptacles at different developmental stages of diploid strawberry (*F. vesca*, 'Ruegen'). SG, small green fruit stage; Wt, white fruit stage; IR, initial red fruit stage; PR, partial red fruit stage; FR, full ripening fruit stage. Relative expression values were relative to receptacles at the SG stage in all cases, which was

assigned an arbitrary value equal to one. Different letters indicate statistically significant differences at $P<0.05$ as determined by Student's t-test.

C. Subcellular localization of FvCSN5A-GFP fusions in transiently transformed *N. benthamiana* leaves. All experiments were assayed 48 h after infiltration. Bars, 20 μm. For the locations of the nuclei, *N. benthamiana* leaves were stained with DAPI. Px-rk/CD3-983 was a marker for the locations of the peroxisome.

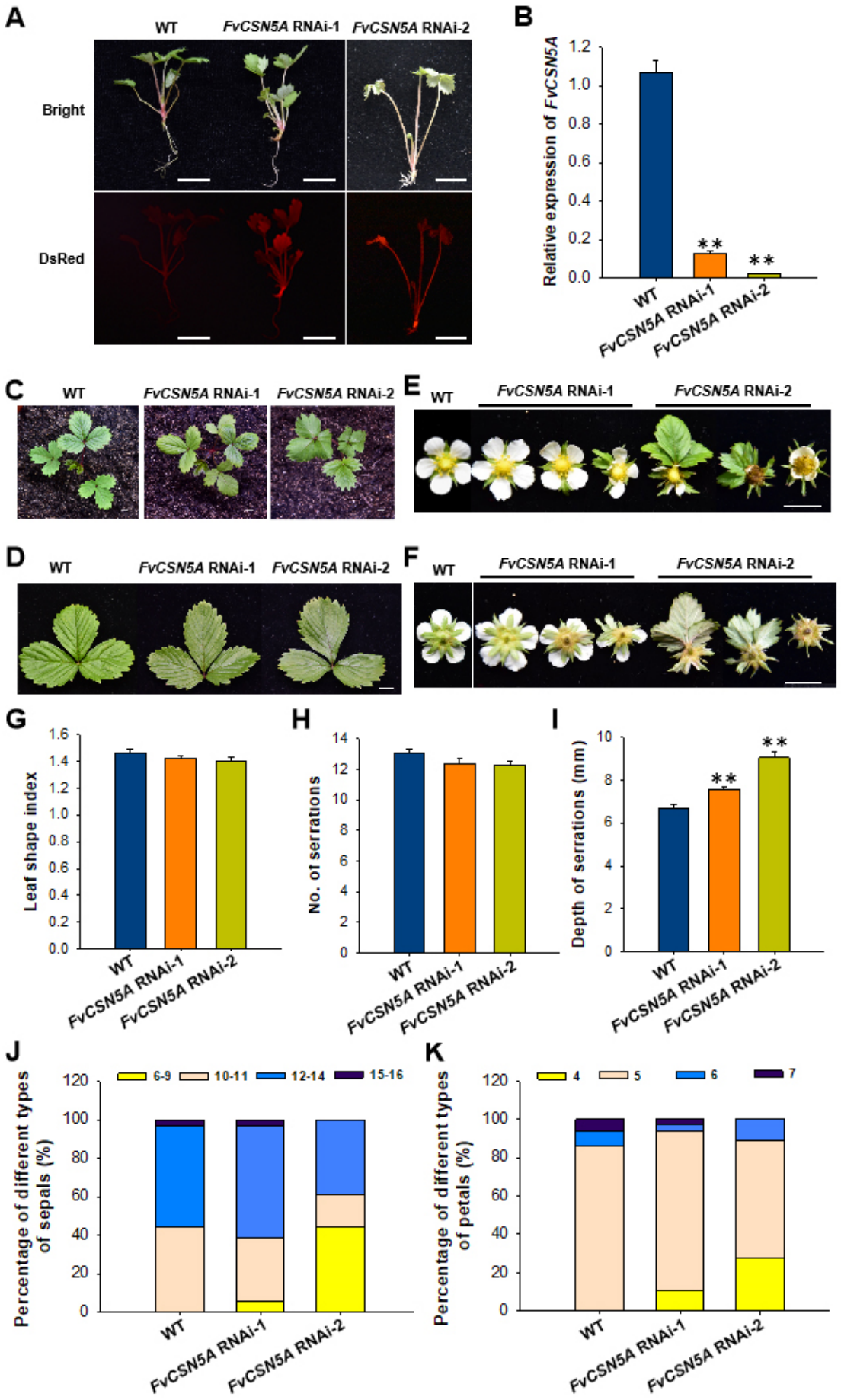
A
WT
FvCSN5A RNAi-1
FvCSN5A RNAi-2
Bright
DsRed
B
Relative expression of FvCSN5A
1.2
1.0
0.8
0.6
0.4
0.2
0.0
**
**
WT
FvCSN5A RNAi-1
FvCSN5A RNAi-2
C
WT
FvCSN5A RNAi-1
FvCSN5A RNAi-2
E
WT
FvCSN5A RNAi-1
FvCSN5A RNAi-2
D
WT
FvCSN5A RNAi-1
FvCSN5A RNAi-2
F
WT
FvCSN5A RNAi-1
FvCSN5A RNAi-2
G
Leaf shape index
1.6
1.4
1.2
1.0
0.8
0.6
0.4
0.2
0.0
WT
FvCSN5A RNAi-1
FvCSN5A RNAi-2
H
No. of serrations
14
12
10
8
6
4
2
0
WT
FvCSN5A RNAi-1
FvCSN5A RNAi-2
I
Depth of serrations (mm)
10
8
6
4
2
0
**
**
WT
FvCSN5A RNAi-1
FvCSN5A RNAi-2
J
Percentage of different types of sepals (%)
6-9
10-11
12-14
15-16
120
100
80
60
40
20
0
WT
FvCSN5A RNAi-1
FvCSN5A RNAi-2
K
Percentage of different types of petals (%)
4
5
6
7
120
100
80
60
40
20
0
WT
FvCSN5A RNAi-1
FvCSN5A RNAi-2

Fig. 3 Phenotypes of the *FvCSN5A* RNAi transgenic plants.

A. Visualization of DsRed accumulation in *FvCSN5A* RNAi plants (right). Bars, 1 cm.

B. Relative expression levels of *FvCSN5A* was determined by RT-qPCR. Statistical significance was determined by Student's t-test. *P < 0.05, **P < 0.01.

C. The photo of wild-type (WT, *F. vesca*, 'Ruegen') and *FvCSN5A* RNAi transgenic plants in soil. Bars, 1 cm.

D. One compound leaf of WT and *FvCSN5A* RNAi transgenic plants. Bars, 1 cm.

E. The flowers of WT and *FvCSN5A* RNAi transgenic plants. Bars, 1 cm.

F. The sepals of WT and *FvCSN5A* RNAi transgenic plants. Bars, 1 cm.

G. Leaf shape index of WT and *FvCSN5A* RNAi transgenic plants.

H. Numbers of the serrations of WT and *FvCSN5A* RNAi transgenic plants.

I. Depth of the serrations of WT and *FvCSN5A* RNAi transgenic plants. **, P < 0.01; Student's t-test.

J. The percentages of different types of sepals in WT and *FvCSN5A* RNAi transgenic plants. n = 36.

K. The percentages of different types of petals in WT and *FvCSN5A* RNAi transgenic plants. n = 36.

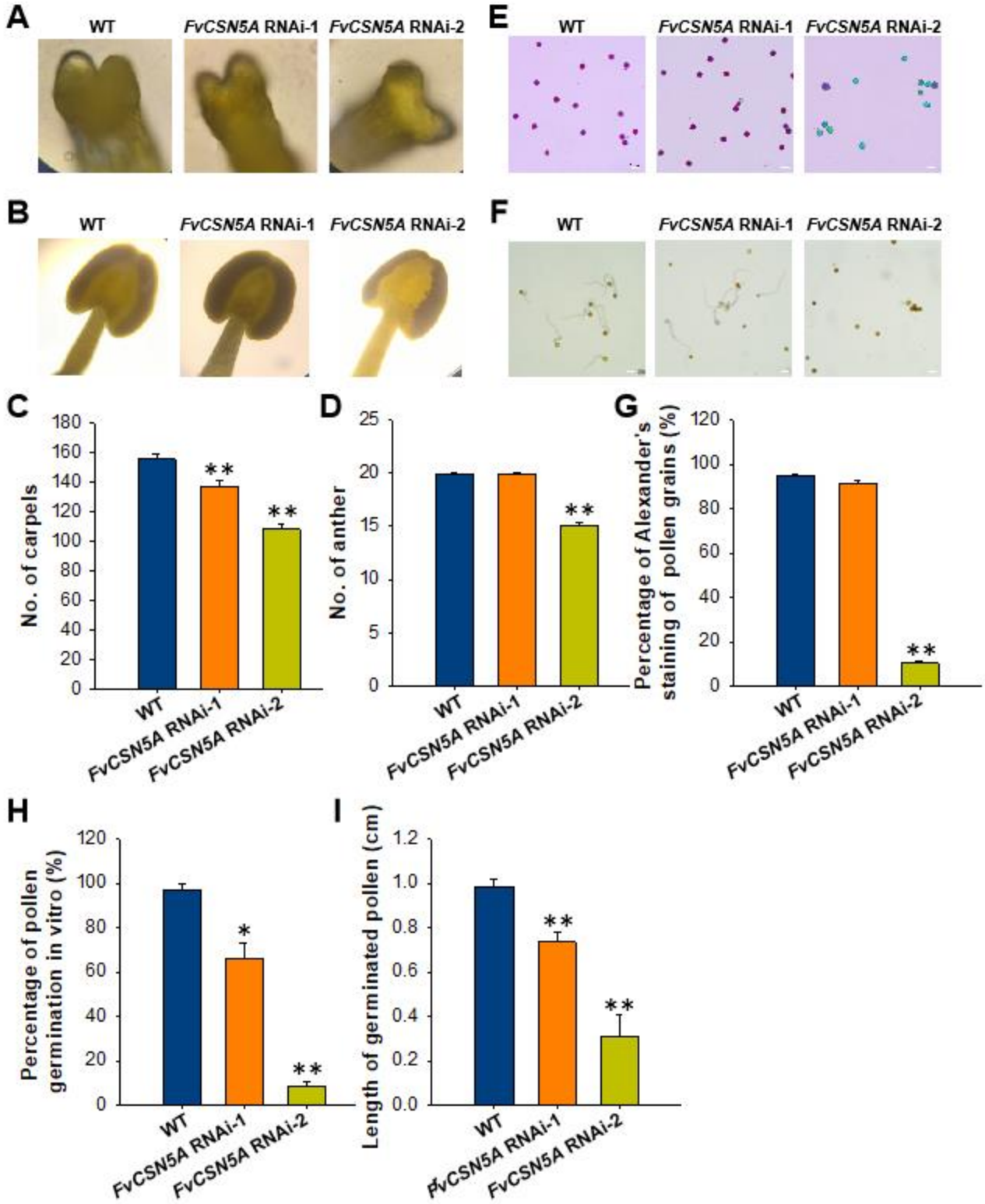

Fig. 4 Pistils and anthers phenotypes of the *FvCSN5A* RNAi transgenic plants.

A-B. The images of pistil (A) and anther (B) of WT and *FvCSN5A* RNAi transgenic plants.

C-D. Numbers of pistil (C) and anther (D) of WT and *FvCSN5A* RNAi transgenic plants. **, $P < 0.01$; Student's t-test.

E. The images showing Alexander's staining of pollen grains from WT and *FvCSN5A* RNAi transgenic plants. The red-stained pollen grains are viable and fertile.

F. The images showing pollen tubes of WT and *FvCSN5A* RNAi transgenic plants germination in *vitro*. Bars, 100 μm.

G. The percentages of Alexander's staining of pollen grains from WT and *FvCSN5A* RNAi transgenic plants. **, $P < 0.01$; Student's t-test.

H. The percentages of WT and *FvCSN5A* RNAi pollen tubes germinated in vitro. *$P < 0.05$; **, $P < 0.01$; Student's t-test.

I. The length of WT and *FvCSN5A* RNAi pollen tubes germinated in vitro. **, $P < 0.01$; Student's t-test.

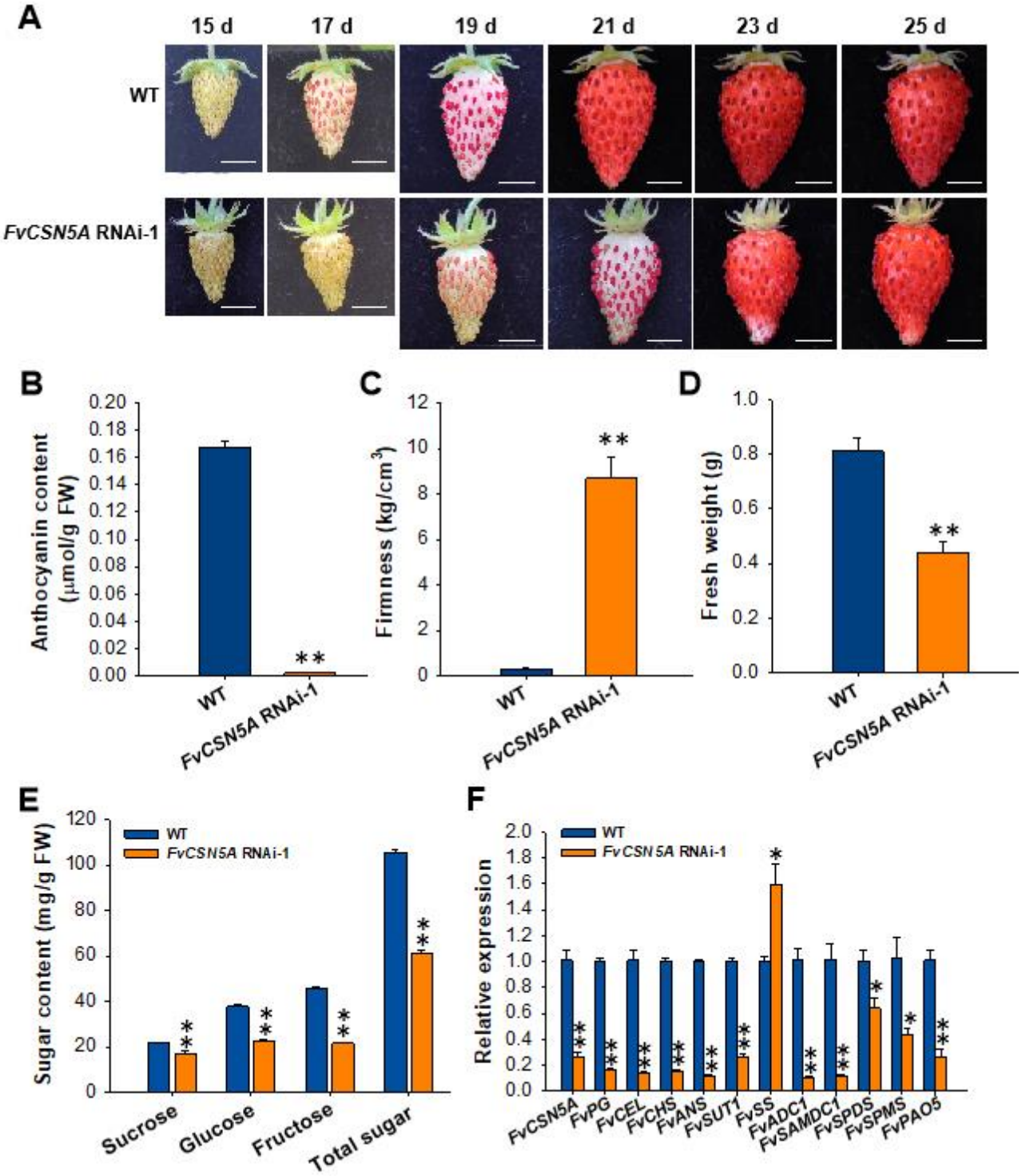

Fig. 5 Fruit ripening changes in *FvCSN5A* transgenic fruits.

A. Photos were taken at 15, 17, 19, 21, 23, and 25 days after pollination respectively to record the fruit phenotype.

B-E. The anthocyanin content (B), firmness (C) fresh weight (D), and soluble sugar content (E) of *FvCSN5A* transgenic and WT fruits. Bars are means SEs of three independent experiments (Student's t-test; **P < 0.01).

F. RT-qPCR was used to analyze the genes' expression in *FvCSN5A* transgenic and WT fruits, and three biological replicates were tested for all samples using the Actin gene from strawberry as an internal control. The relative expression levels were calculated using the $2^{-\triangle\triangle Ct}$ method. FvCSN5A: COP9 Signalosome5; FvPG: polygalacturonase; FvCEL: cellulose; FvCHS: chalcone synthase; FvANS: anthocyanidin synthase; FvSUT1: sucrose transporter1; FvSS: sucrose

synthase. FvADC1: arginine decarboxylase1; FvSAMDC1: S-adenosyl-methionine decarboxylase1; FvSPDS1: spermidine synthase1; FvSPMS: spermine synthase; FvPAO5: polyamine oxidase5. *P < 0.05; **, P < 0.01; Student's t-test.

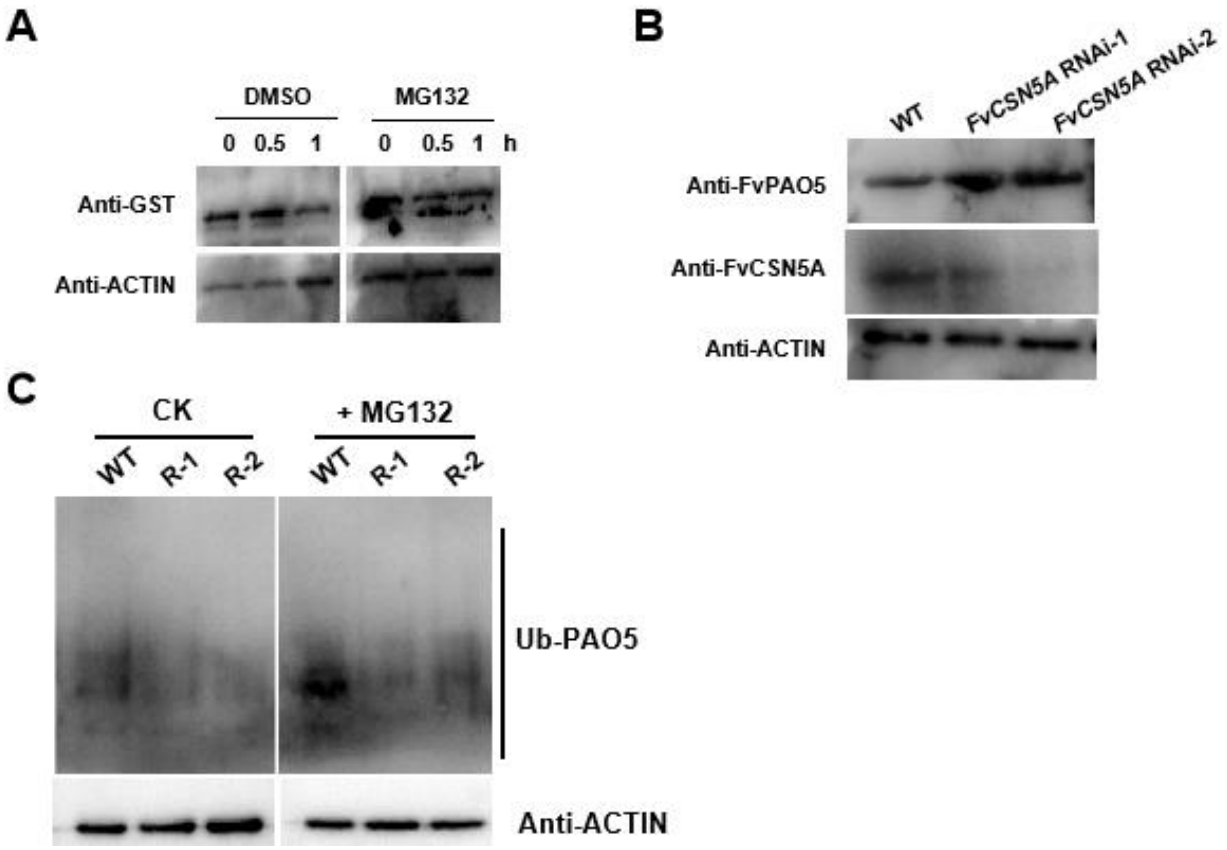

Fig. 6 The ubiquitination degradation of FvPAO5 is dependent on FvCSN5A.

A. Cell free FvPAO5 protein degradation. Total protein was extracted from strawberry leaves and incubated with FvPAO5-GST protein for 0.5, and 1 h with MG132 treatment or DMSO treatment as a control. FvPAO5-GST protein and Total plant protein were detected by Anti-GST and Anti-ACTIN, respectively.

B. FvPAO5 and FvCSN5A protein aboundance detection in *FvCSN5A* RNAi and WT plants. FvPAO5 and FvCSN5A were detected by Anti-FvPAO5 and Anti- FvCSN5A, respectively.

C. In vivo FvPAO5 polyubiquitination in *FvCSN5A* RNAi and WT plants. Three-month-old seedlings were transferred to MS medium supplemented with or without 50 μM MG132 for 5 h and then harvested for protein extraction. Each total protein was incubated with P62-agarose to obtain ubiquitinated proteins. Polyubiquitinated FvPAO5 was detected with an anti- FvPAO5 antibody. The accumulation of ACTIN in the total protein was tested as a control.

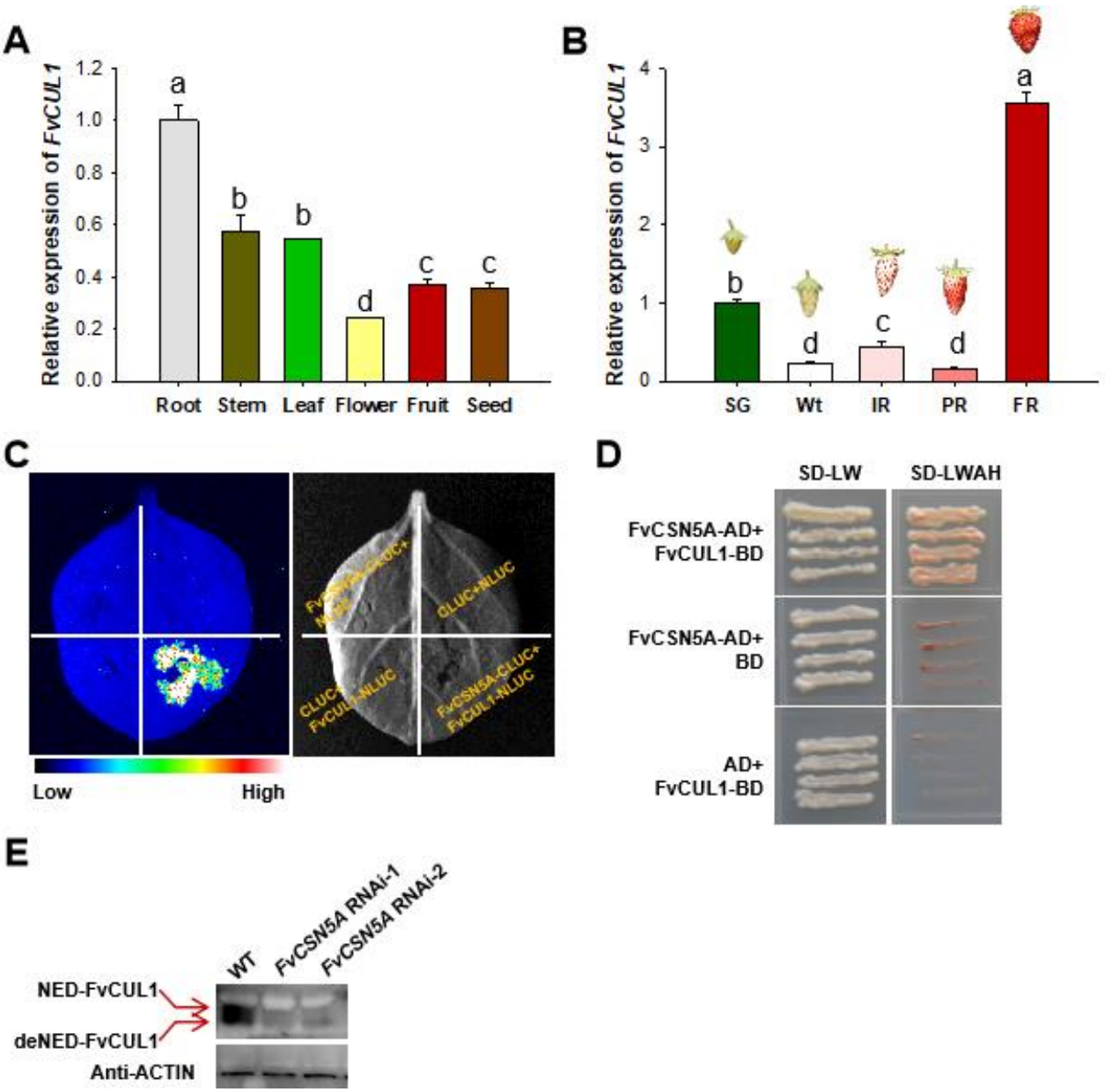

Fig. 7 FvCUL1 interacted with FvCSN5A in vitro and in vivo.

A. The transcript level of *FvCUL1* in different tissues of strawberry. Different letters indicate statistically significant differences at P<0.05 as determined by Student's t-test.

B. *FvCUL1* transcript levels in fruit receptacles at different developmental stages of diploid strawberry. Different letters indicate statistically significant differences at P<0.05 as determined by Student's t-test.

C. FvCUL1 interacted with FvCSN5A in FLC assay. The CDS of *FvCSN5A* was constructed into pCAMBIA1300-CLUC vector, and the CDS of *FvCUL1* was constructed into pCAMBIA1300-NLUC vector.

D. FvCUL1 interacted with FvCSN5A in yeast two-hybrid assay. SD-LW: synthetic dropout medium without Leu and Trp; SD-LWHA: synthetic dropout medium without Leu, Trp, His, and Ade.

E. Detection of FvCUL1 protein in *FvCSN5A* RNAi and WT plants using antibody Anti-CUL1. NED- FvCUL1: FvCUL1 with neddylation; deNED- FvCUL1: FvCUL1 without neddylation.

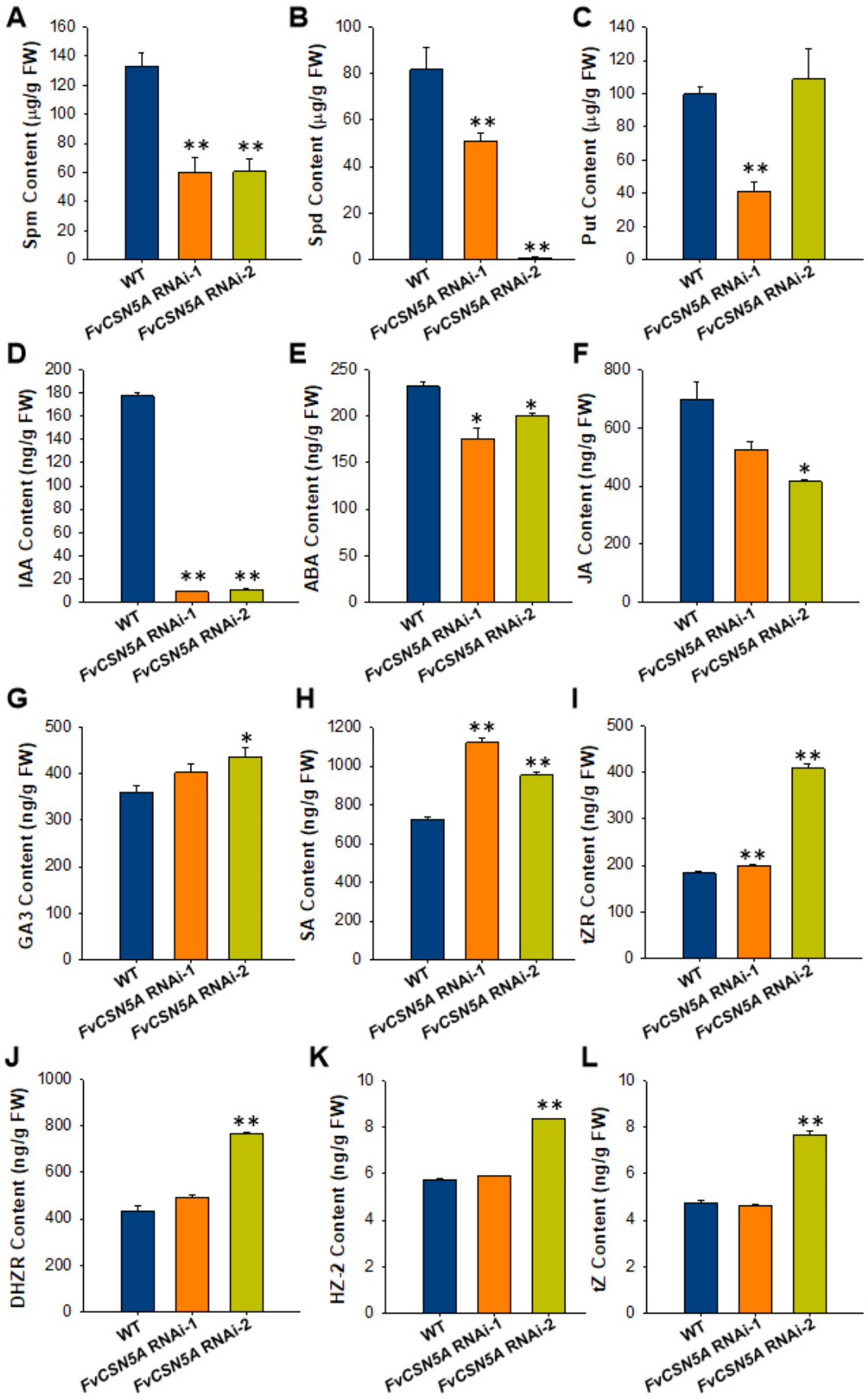
A
Spm Content (μg/g FW)
B
Spd Content (μg/g FW)
C
Put Content (μg/g FW)
D
IAA Content (ng/g FW)
E
ABA Content (ng/g FW)
F
JA Content (ng/g FW)
G
GA3 Content (ng/g FW)
H
SA Content (ng/g FW)
I
tZR Content (ng/g FW)
J
DHZR Content (ng/g FW)
K
HZ-2 Content (ng/g FW)
L
tZ Content (ng/g FW)
WT
FvCSN5A RNAi-1
FvCSN5A RNAi-2

1003

Fig. 8 Polyamine and phytohormone content in *FvCSN5A* RNAi transgenic plants

A-C: Spd (A), Spm (B), and Put (C) content in WT and *FvCSN5A* RNAi transgenic leaves.

D-L. Phytohormone IAA, ABA, JA, GA3, SA, tZR, DHZR, HZ-2 and tZ content in WT and *FvCSN5A* RNAi transgenic leaves. *P < 0.05; **, P < 0.01; Student's t-test.

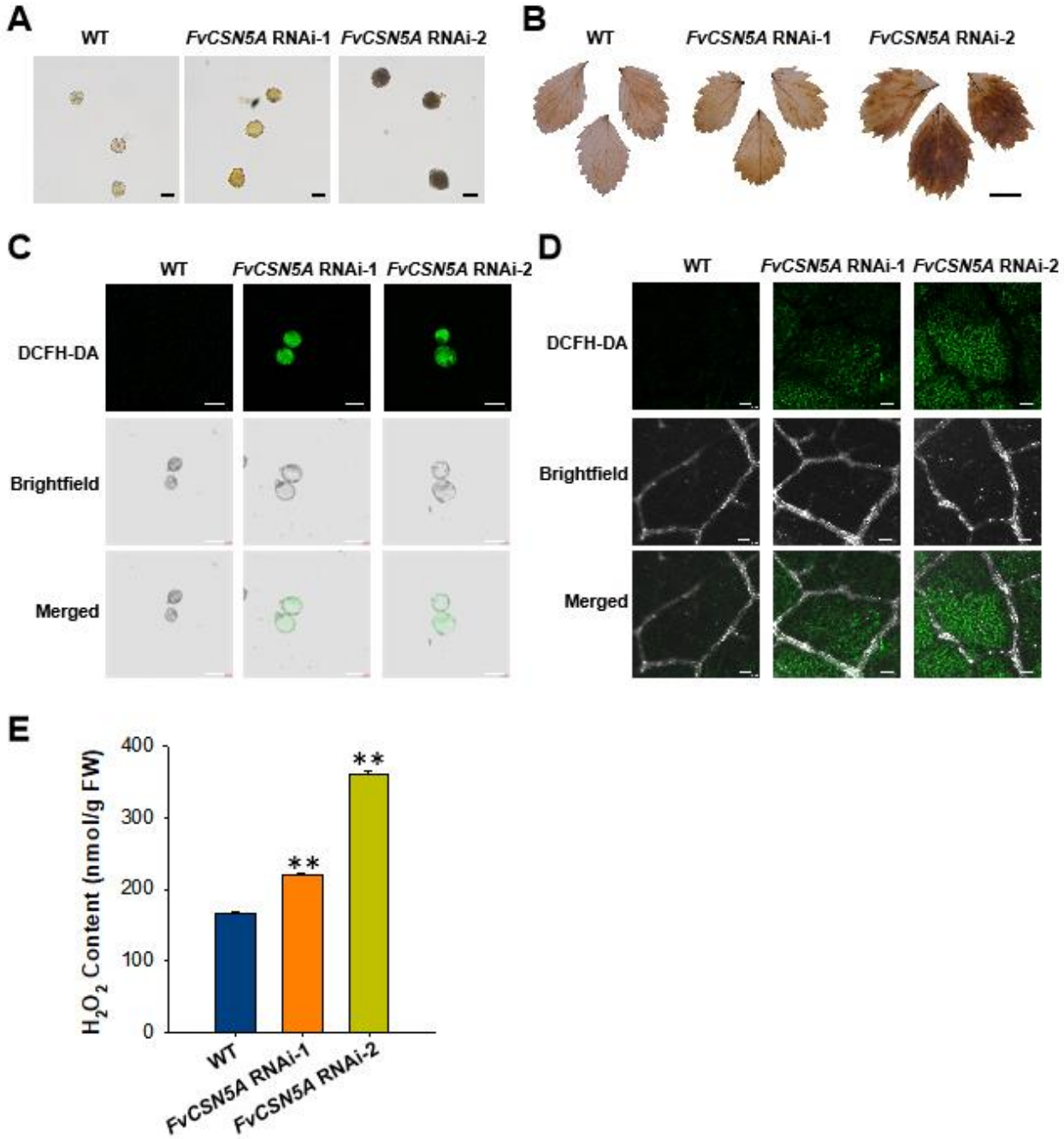

Fig. 9 Detection of ROS accumulation in *FvCSN5A* RNAi transgenic plants

A. DAB dye of pollen grains from *FvCSN5A* RNAi and WT plants. Bars, 50 μm.

B. DAB dye of one compound leaf from *FvCSN5A* RNAi and WT plants. Bars, 1cm.

C. ROS signal of pollen grains determinated by DCFH-DA. Bars, 20 μm.

D. ROS signal of leaf determinated by DCFH-DA. Bars, 50 μm.

E. The content of H_2O_2 in *FvCSN5A* RNAi transgenic plants and WT.

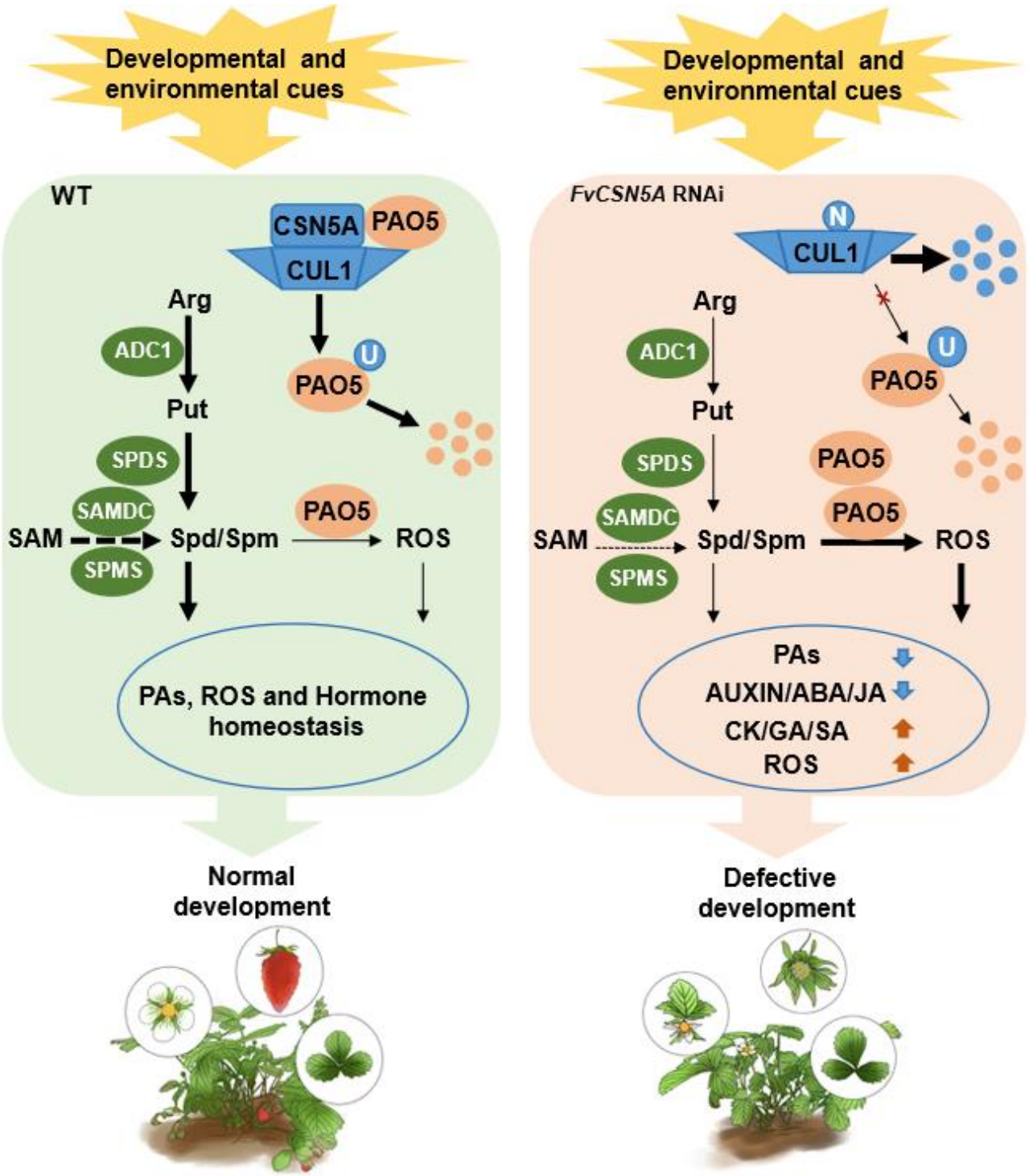

Fig. 10 proposed working model

An equilibrium regulation for the composition and content of Put, Spd and Spm, is programmed by PA biosynthesis and degradation: Put-related key enzymes is ADC1; Spd/Spm-related key enzymes include SAMDC1, SPDS, and SPDM for biosynthesis and PAO5 for degradation. In response to environments, the two equilibria from Put/Spd/Spm metabolism to vegetative/reproductive growth are fine-tuned at transcripts, translation and post-translation for plant better growth and breeding. The CSN5A interacting with CUL1 mediates degradation of PAO5, not only rapidly controlling PA balance,

but also H_2O_2 production, which could be integrated into various hormones. Finally, PAs, ROS and hormones synergistically regulates strawberry development and adaptation.

CSN5A is essential for the deneddylation of CUL1, which may affect the protein stability of CUL1 and SCF E3 ubiquitin ligase activity. CUL1 protein level in the *FvCSN5A* RNAi markedly decreases, and PAO5 increases. These changes lead to the significant decrease of PA, auxin, ABA, JA content, and excessive accumulation of H_2O_2. The homeostasis disruption in *FvCSN5A* RNAi plants may be responsible for the growth defects, slow fruit ripening and poor fertility phenotype.

Supplemental files

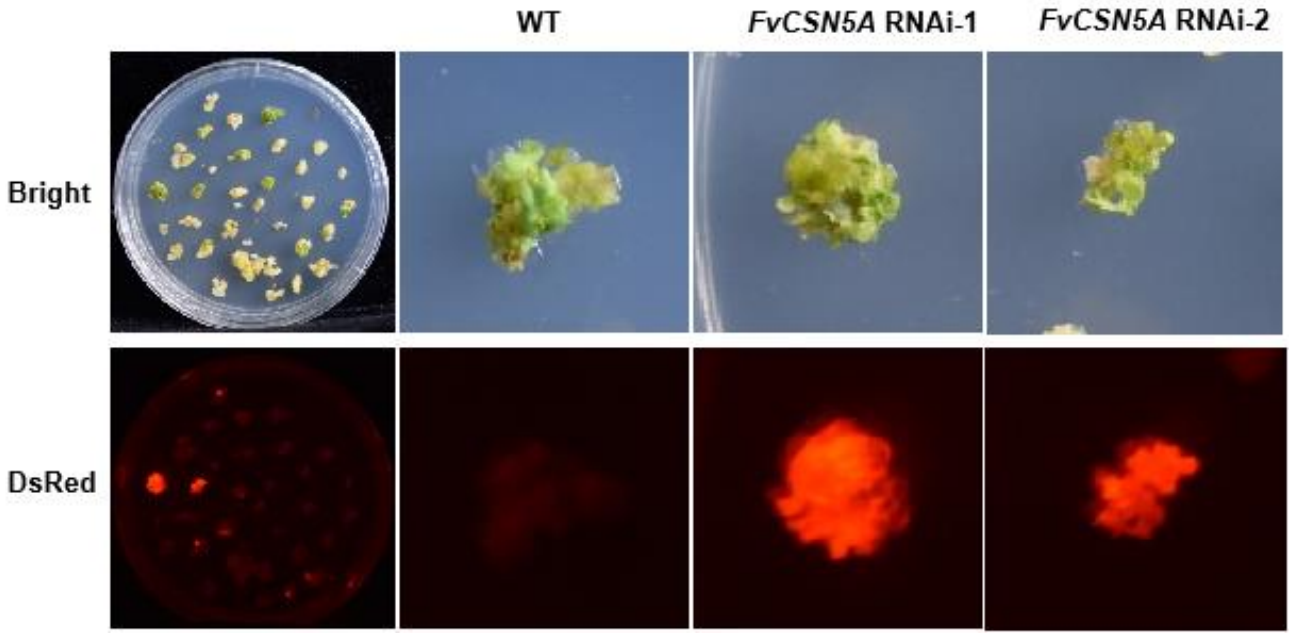

Supplemental Fig. 1 *FvCSN5A* RNAi transgenic callus screening.
The red calluses were *FvCSN5A* RNAi successful transgenic callus, which were named *FvCSN5A* RNAi-1 and *FvCSN5A* RNAi-2.

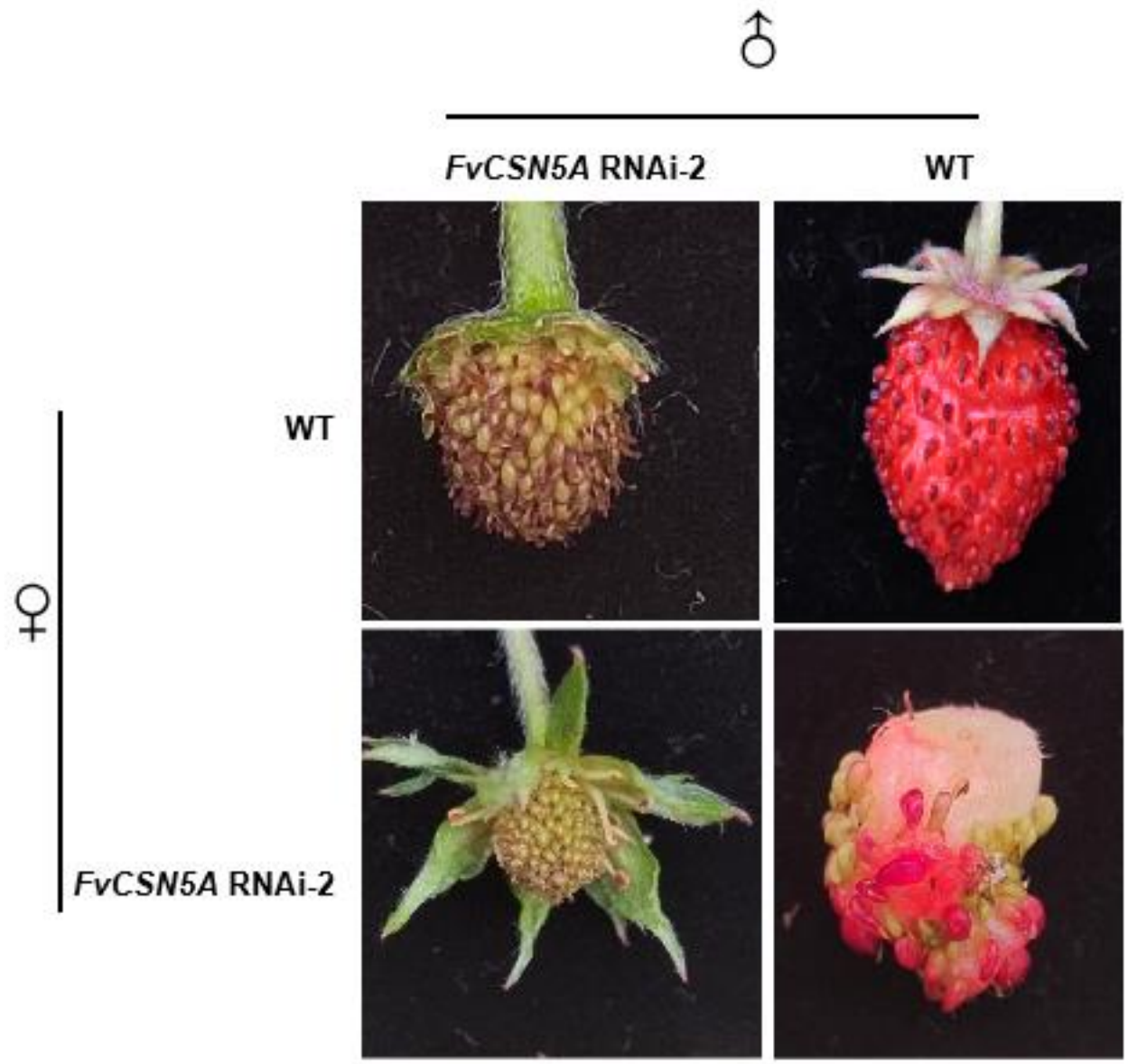

Supplemental Fig. 2 Reciprocal crosses between WT and *FvCSN5A* RNAi -2 plant

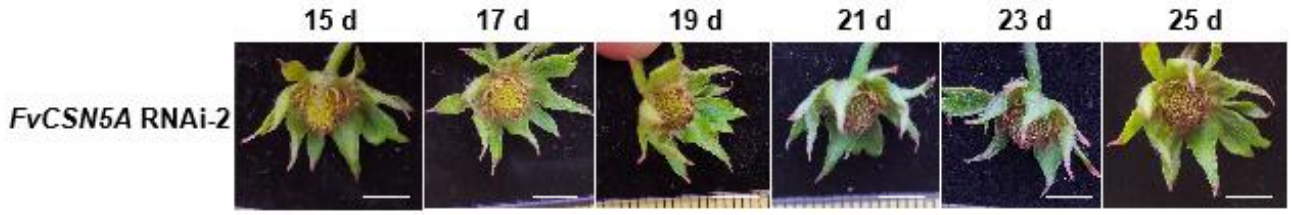

Supplemental Fig. 3 Observation of fruit development process of *FvCSN5A* RNAi-2 transgenic plant.

Photos were taken at 15, 17, 19, 21, 23, and 25 days after pollination to record the fruit phenotype. Bars, 0.5 cm.

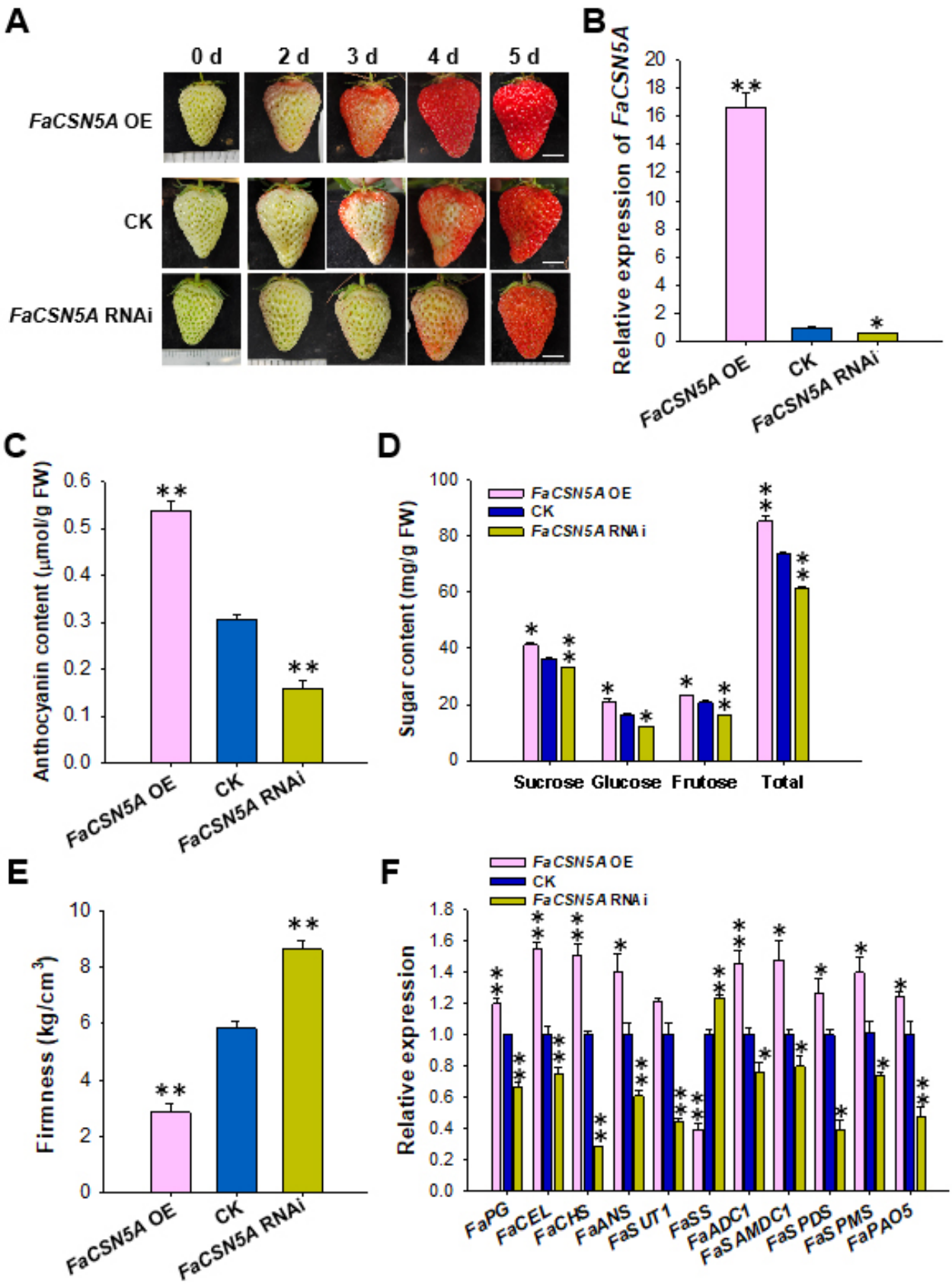

Supplemental Fig. 4 Manipulation of *FaCSN5A* expression affected physiological parameters and transcript levels of ripening-related genes.

A. Phenotypes of *FaCSN5A* OE and *FaCSN5A* RNAi strawberry fruits. Agrobacterium GV3101 strains containing RNAi or overexpression FaVPT1 recombinant plasmids were injected into DG fruits attached to the plant. The fruit phenotype was recorded at 0, 2, 3, 4, and 5 days after injection. Bars, 1 cm.

B. Analysis of *FaCSN5A* transcript levels in *FaCSN5A* OE and *FaCSN5A* RNAi fruits compared with the control. *P < 0.05; **, P < 0.01; Student's t-test.

C-E. The anthocyanin content (C), soluble sugar content (D), and firmness (E) of *FaCSN5A* OE and *FaCSN5A* RNAi strawberry fruits. **, P < 0.01; Student's t-test.

F. RT-qPCR was used to analyze the genes' expression in *FaCSN5A* OE and *FaCSN5A* RNAi fruits. Relative expression levels were calculated using the $2^{-\triangle\triangle Ct}$ method. FaPG: polygalacturonase; FaCEL: cellulose; FaCHS: chalcone synthase; FaANS: anthocyanidin synthase; FaSUT1: sucrose transporter1; FaSS: sucrose synthase. FaADC1: arginine decarboxylase1; FaSAMDC1: S-adenosyl-methionine decarboxylase1; FaSPDS1: spermidine synthase1; FaSPMS: spermine synthase; FaPAO5: polyamine oxidase5. *P < 0.05; **, P < 0.01; Student's t-test.

Supplemental Table S1. Oligonucleotide sequences of the primers used in this study.

Primer Name	Sequence (5'-3')	Destination
CSN5-AD-F	GCCATGGAGGCCAGTGAATTCATGGATGCGGAAATAGCGC	Y2H
CSN5-AD-R	CAGCTCGAGCTCGATGGATCCACTTTCAATCATTGGCTCAGGG	Y2H
PAO5-BD-F	ATGGCCATGGAGGCCGAATTCATGGTGGCCAAGAAACCAAG	Y2H
PAO5-BD-R	ATGCGGCCGCTGCAGGTCGACAACCCCAACATGGTGGTTG	Y2H
CUL1-BD-F	TCAGAGGAGGACCTGCATATG ATGGAGCGCAAGATTATCGAGTTG	Y2H
CUL1-BD-R	TCGACGGATCCCCGGGAATTC TGCAAGGTACTTGAACGTGTTCG	Y2H
CSN5-His-F	ATGGGTCGCGGATCCGAATTCATGGATGCGGAAATAGCGC	Protein purification
CSN5-His-R	TGCGGCCGCAAGCTTGTCGACACTTTCAATCATTGGCTCAGGG	Protein purification
PAO5-GST-F	CCGCGTGGATCCCCGGAATTCATGGTGGCCAAGAAACCAAG	Protein purification
PAO5-GST-R	GATGCGGCCGCTCGAGTCGACAACCCCAACATGGTGGTTG	Protein purification
CSN5-CCLUC-F	ACGGGGGACGAGCTCGGTACCATGGATGCGGAAATAGCGC	FLC
CSN5-CCLUC-R	CGCGTACGAGATCTGGTCGACACTTTCAATCATTGGCTCAGGG	FLC
PAO5-NLUC-F	ACGGGGGACGAGCTCGGTACCATGGTGGCCAAGAAACCAAG	FLC
PAO5-NLUC-R	CGCGTACGAGATCTGGTCGAC AACCCCAACATGGTGGTTG	FLC
FvCUL1-NLUC-F	5'-ACGGGGGACGAGCTCGGTACC ATGGAGCGCAAGATTATCGAGT	FLC
FvCUL1-NLUC-R	5'-CGCGTACGAGATCTGGTCGACTGCAAGGTACTTGAACGTGTTC	FLC
CSN5-YCE-F	TGGCGCGCCACTAGTGGATCCATGGATGCGGAAATAGCGC	BiFC
CSN5-YCE-R	CCCGGGAGCGGTACCCTCGAGACTTTCAATCATTGGCTCAGGG	BiFC
PAO5-YNE-F	TGGCGCGCCACTAGTGGATCCATGGTGGCCAAGAAACCAAG	BiFC
PAO5-YNE-R	CCCGGGAGCGGTACCCTCGAGAACCCCAACATGGTGGTTG	BiFC
CSN5-1300-GFP-F	GGTCGACATTTAAATACTAGTATGGATGCGGAAATAGCGC	CoIP/OE
CSN5-1300-GFP-R	GCCCTTGCTCACCATGGTACCACTTTCAATCATTGGCTCAGGG	CoIP/OE
PAO5-1300-GFP-F	GGTCGACATTTAAATACTAGTATGGTGGCCAAGAAACCAAG	CoIP/OE
PAO5-1300-GFP-R	GCCCTTGCTCACCATGGTACCAACCCCAACATGGTGGTTG	CoIP/OE
CSN5-MYC-F	GGTCGACATTTAAATACTAGTATGGATGCGGAAATAGCGC	CoIP
CSN6-MYC-R	GCCCTTGCTCACCATGGTACCACTTTCAATCATTGGCTCAGGG	CoIP
CSN5-RNAi-F	GGGGACAAGTTTGTACAAAAAAGCAGGCTTCCCATCTTCTACTACGACGAGGC	RNAi
CSN5-RNAi-R	GGGGACCACTTTGTACAAGAAAGCTGGGTCTGCCTGTTTGTTAGTCTGGGAA	RNAi
Actin-RT-F	GCCAACCGTGAGAAGATG	RT-qPCR
Actin-RT-R	TCCAGAGTCAAGAACAATACCAG	RT-qPCR
CSN5-RT-F	TATTCCCAGACTAACAAACAGGC	RT-qPCR
CSN5-RT-R	GAGTGGGGTCAATAACAACAGCC	RT-qPCR
PAO5-RT-F	CGGATTGAGATGGGTGCTACTTG	RT-qPCR
PAO5-RT-R	AATGGTCTTGGCTTCGTCTGATG	RT-qPCR
CUL1-RT-F	GTTGGATCAAGGATGGGACT	RT-qPCR
CUL1-RT-R	TTGGGAATAGTCATACGGGG	RT-qPCR
PG-RT-F	GCAAGTAGAGTCGCACAGTTTT	RT-qPCR
PG-RT-R	TCAGTATTAGGCTTCCCACCA	RT-qPCR
CEL-RT-F	GCTCTGTTTTGCCTGGACTT	RT-qPCR
CEL-RT-R	GCGTGGCTTAGATAGTTGGAAT	RT-qPCR
CHS-RT-F	CATACCCCGACTACTACTTTCGT	RT-qPCR
CHS-RT-R	CGCACATACTGGGATTCTCTT	RT-qPCR

ANS-RT-F	CTTGGCTTGGGATTAGAAGAAG	RT-qPCR
ANS-RT-R	TGAGGGCATTTTGGGTAGTAGT	RT-qPCR
SUT1-RT-F	TTCAAGCGACAGAAATACCC	RT-qPCR
SUT1-RT-R	ACCCAATCCAGTTTAGACCAG	RT-qPCR
SS-RT-F	TTATCCCTCGCATTCTTATT	RT-qPCR
SS-RT-R	CAATTCCCTTCTCGGTTCTA	RT-qPCR

1067